Proglucagon signalling in the rat Dorsomedial Hypothalamus – Physiology and high-fat diet-mediated alterations

A.M. Sanetra [a,*], K. Palus-Chramiec [a], L. Chrobok [a,b], J.S. Jeczmien-Lazur [a], J.D. Klich [a,c], M. H. Lewandowski [a,*]

[a] Department of Neurophysiology and Chronobiology, Institute of Zoology and Biomedical Research, Jagiellonian University in Krakow, Gronostajowa Street 9, 30-387 Krakow, Poland
[b] School of Physiology, Pharmacology, and Neuroscience, University of Bristol, University Walk, Biomedical Sciences Building, Bristol BS8 1TD, UK
[c] Max-Delbrück-Center for Molecular Medicine in the Helmholtz Association (MDC), Robert-Rössle Street 10, 13125 Berlin, Germany

ABSTRACT

A relatively new pharmacological target in obesity treatment has been the preproglucagon (PPG) signalling, predominantly with glucagon-like peptide (GLP) 1 receptor agonists. As far as the PPG role within the digestive system is well recognised, its actions in the brain remain understudied. Here, we investigated PPG signalling in the Dorsomedial Hypothalamus (DMH), a structure involved in feeding regulation and metabolism, using in situ hybridisation, electrophysiology, and immunohistochemistry. Our experiments were performed on animals fed both control, and high-fat diet (HFD), uncovering HFD-mediated alterations. First, sensitivity to exendin-4 (Exn4, a GLP1R agonist) was shown to increase under HFD, with a higher number of responsive neurons. The amplitude of the response to both Exn4 and oxyntomodulin (Oxm) was also altered, diminishing its relationship with the cells' spontaneous firing rate. Not only neuronal sensitivity, but also GLP1 presence, and therefore possibly release, was influenced by HFD. Immunofluorescent labelling of the GLP1 showed changes in its density depending on the metabolic state (fasted/fed), but this effect was eliminated by HFD feeding. Interestingly, these dietary differences were absent after a period of restricted feeding, allowing for an anticipation of the alternating metabolic states, which suggests possible prevention of such outcome.

1. Introduction

Increasing prevalence of obesity along with its multiple pathophysiological consequences have resulted in an urgent need for both treatment and prevention options. Amongst various treatment attempts, promising results have been obtained with analogues of glucagon-like peptides (GLP; for a review see Trujillo et al., 2021). These include GLP1 and GLP2, which are posttranslationally cleaved from preproglucagon (PPG) by prohormone convertases (PC 1/3 or PC 2), also producing oxyntomodulin (Oxm), glucagon, miniglucagon or glicentin (Bataille and Dalle, 2014). The PPG peptide family are responsible for glucose homeostasis, with a recognised and widely exploited potential in the treatment of both types of diabetes (Kolterman et al., 2003; Dupré et al., 2004). However, they are also potent satiety signals influencing behaviour (decreasing food intake), and metabolism (stimulating energy expenditure; Hwa et al., 1998, Dakin et al., 2001, 2002, Baggio et al., 2004, Osaka et al., 2005, Wynne et al., 2006, Pocai et al., 2009, Kosinski et al., 2012). These properties make them an interesting therapeutical target for obesity, however, they are mediated by the central nervous system, which in comparison to the digestive system has been hugely

underexplored in the context of PPG signalling.

The main central source of PPG is located in the brainstem Nucleus of the Solitary Tract (NTS, Larsen et al., 1997). NTS PPG neurons send projections to various brain sites including the Dorsomedial Hypothalamus (DMH; Renner et al., 2012), which expresses receptors for both GLP1 (Merchenthaler et al., 1999; Tang-Christensen et al., 2001; Cork et al., 2015; Lee et al., 2018; Maejima et al., 2021) and GLP2 (Tang-Christensen et al., 2000, 2001). Furthermore, amongst the hypothalamic regions, the DMH shows the highest susceptibility to diet-induced obesity (DIO, Zhang et al., 2020), which includes overexpression of the GLP1 receptor (GLP1R), binding both GLP1 and Oxm. We have also recently shown that high-fat diet (HFD; a rodent model of obesity, Winzell and Ahrén, 2004) disrupts the day/night rhythm in the neuronal activity of DMH cells down to the level of their electrophysiological properties (Sanetra et al., 2022a, 2022b) even before the development of obesity. Therefore, as a next step, we performed a complex analysis of GLP1, GLP2 and Oxm actions in the DMH, with a separation into three main sections: GLP1 and GLP2 receptor expression, neuronal sensitivity to the peptides of interest, and their abundance in different conditions.

First, in situ hybridisation was used to detect *Glp1r* and *Glp2r* mRNA and investigate their spatial distribution, as well as HFD-induced changes in their expression. Next, using ex vivo electrophysiology we recorded changes in the neuronal sensitivity to the PPG-derived peptides between light and dark phases of the 24 h cycle. Finally, as a representative of all three co-released substances we investigated the GLP1 immunoreactivity in the DMH under different metabolic states – fasted and fed, occurring either unpredictably, or after a period of time-restricted feeding. Here, we observed lower density of GLP1 immunoreactivity in hungry animals, but only for non-anticipated fasted state.

All protocols were performed on animals fed control (CD), or high-fat diet (HFD) for no longer than 4 weeks, in order to study potential HFD-evoked changes to the PPG signalling, developing even before the onset of obesity, at the time when the DMH circadian rhythmicity is already being altered (Sanetra et al., 2022a, 2022b). Our data show that short-term HFD impacts DMH neuronal responsiveness to Oxm and exendin-4 (Exn4, a selective GLP1R agonist), completely abolishing its dependence on the spontaneous activity. Furthermore, HFD-induced changes in the amount of GLP1 in various subdivisions of the DMH (compact – cDMH, dorsal – dDMH and ventral – vDMH), suppress its relationship with the metabolic state of the animal, indicating an uncoupling between peripheral and central regulators of metabolism. Finally, no difference between the diets occurs under restricted feeding (RF), when GLP1 immunoreactivity remains constant throughout the feeding cycle.

2. Materials and methods

2.1. Animal maintenance

All experiments were carried out in accordance with the Polish Animal Welfare Act of 23 May 2012 (82/2012) and the European Communities Council Directive (86/609/EEC), and had received approval from the Local Ethics Committee in Krakow (No. 18/2018, 349/2022).

Animals used in the study were male Sprague-Dawley (SD) rats, bred at the animal facility of the Institute of Zoology and Biomedical Research, Jagiellonian University in Krakow (Poland). Females were excluded due to probable interactions between the oestrous cycle and metabolism, especially during puberty. Rats were kept in constant environmental conditions (temperature ~ 23 °C, humidity ~ 65 %) and standard lighting conditions (LD 12:12), with water supplied ad libitum, and food supplied either also ad libitum or accordingly to the experimental protocols, as described in the following sections.

At the age of weaning (4 weeks), the animals were assigned to either control or experimental group. The first one was fed control diet (CD; ~ 3514 kcal/kg, fat content 4 %, energy from: 10 % fat, 24 % protein, 66 % carbohydrates, cat. no. C1090–10; Altromin International, Germany), whereas the experimental group received HFD (~ 5389 kcal/kg, fat content 42 %, energy from: 70 % fat, 16 % protein, 14 % carbohydrates, cat. no. C1090–70; Altromin International). Animals were maintained on the assigned diet until the end of the experiment (between 2 and 4 weeks).

2.2. In situ hybridisation

2.2.1. Tissue preparation

For the in situ hybridisation 6 rats (3 per diet) were used, after 4 weeks on a respective diet. The animals were sacrificed in the middle of the light phase (zeitgeber time - ZT6, where ZT0 is the onset of the light phase) by isoflurane inhalation (1 ml in the incubation chamber, Baxter, USA) followed by decapitation. Brains were quickly extracted, frozen on dry ice and stored at −80 °C. Sections including the DMH were cut on a cryostat (Leica CM1950, Germany) at −20 °C and thaw-mounted on Superfrost-Plus slides (Fisher Scientific, USA). Slices were then fixed for 15 min in a 4 % paraformaldehyde solution (PFA) in phosphate-buffered saline (PBS), rinsed in PBS (2 × 1 min), dehydrated in ethanol solutions of increasing concentrations (50 %, 70 % and 2 × 100 %, 5 min in each) and circled with a hydrophobic marker.

2.2.2. RNAscope assay

The assay was performed with the RNAscope multiplex in situ hybridization protocol (Advanced Cell Diagnostics—ACD, USA), which started with a 12-min long pre-treatment with protease IV. Next, the slides were rinsed in PBS (2 × 1 min) and incubated with probes targeting *Glp1r* and *Glp2r* (2 h at 40 °C). After that, the slides were rinsed in wash buffer (2 × 2 min) and a four-step-long signal amplification protocol was applied (3 × 30 min with AMP1–3 and 15 min with fluorophores: Atto 647 for *Glp1r* and Atto 550 for *Glp2r*, all at 40 °C). Following, the slides were rinsed again in wash buffer (2 × 2 min), and coverslipped with DAPI.

2.2.3. Image processing and analysis

Microphotographs were taken with an epifluorescence microscope (Axio Imager M2, Zeiss, Germany) and visualised in ZEN software (ZEN 2.5. blue edition, Zeiss), where *Glp1r*-positive neurons were manually counted, for each part of the DMH separately, and divided by the substructure area to obtain the density. Both probes, were also analysed as the density of the fluorescent signal, reflecting *Glp1r/Glp2r* mRNA abundance. For this, stacks were processed into a maximum intensity projection in ZEN 2.3. (black edition, Zeiss), followed by contrast enhancement and maxima count in ImageJ software (NIH, USA; Fiji: Schindelin et al., 2012).

2.3. Electrophysiology

2.3.1. Tissue preparation

All electrophysiological recordings were performed either during the day (cull between ZT1–3, recording starting at ZT6 ± 1 h) or at night (cull at ZT13–15, recording starting at ZT18 ± 1 h). Recording time never exceeded the end of the projected lighting phase (ZT12 for daytime or ZT24 for nighttime recordings).

After 2–4 weeks on a diet, the animals were anaesthetized with isoflurane (1 ml in the incubation chamber, Baxter) and sacrificed by decapitation. The brains were quickly removed and cut into 250 μm thick coronal slices containing the DMH with a vibroslicer (Leica VT1000S). Throughout the entire procedure, the brains were immersed in ice-cold, cutting artificial cerebro-spinal fluid (cACSF), containing (in mM): 25 $NaHCO_3$, 3 KCl, 1.2 Na_2HPO_4, 2 $CaCl_2$, 10 $MgCl_2$, 10 glucose, 125 sucrose with addition of a pH indicator, Phenol Red 0.01 mg/l, osmolality ~ 290 mOsmol/kg, continuously carbogenated (95 % O_2, 5 % CO_2). Before the start of the recoding, the slices were incubated for at least half an hour (MEA) or 2 h (patch clamp) in the recording artificial cerebro-spinal fluid (rACSF), containing: (in mM): 125 NaCl, 25 $NaHCO_3$, 3 KCl, 1.2 Na_2HPO_4, 2 $CaCl_2$, 2 $MgCl_2$, 5 glucose and 0.01 mg/l

of Phenol Red (initial temperature: 32 °C, cooled to room temperature).

2.3.2. Multi-electrode array recordings

2.3.2.1. Recording.
Multi-electrode array recordings (MEA) were performed on a total of 17 animals (CD daytime: 3, HFD daytime: 3, CD nighttime: 5, HFD nighttime: 6), using MEA2100-System (Multichannel Systems GmbH, Germany; Belle et al., 2021). DMH-containing brain slices were placed on an 8 × 8 perforated electrode matrix (60pMEA100/30iR-Ti, Multichannel Systems), which ensured electrode coverage of the entire structure. Double perfusion system of the recording chamber was used, with the top circuit used for constant perfusion with fresh rACSF as well as drug application, and the bottom circuit crucial for establishing slight pressure sucking the slices into proximity with the recording electrodes. At least half an hour was waited for the set up to stabilise, after which the recordings started with another half an hour of baseline recording. Then, proglucagon-derived peptides were applied, one at a time, with at least an hour between consecutive applications, after the responding cells had fully recovered from the previous effect.

Signal was acquired with Multi Channel Experimenter software (Multichannel Systems), with a sampling frequency of 20 kHz.

2.3.2.2. Data analysis.
Single-unit activity analysis was employed in order to quantify the percentage of responsive cells, and evaluate possible changes in the amplitude of the effect between the groups.

Multi Channel DataManager (Multichannel Systems GmbH) was used to export raw signal into HDF5 and CED-64 files. The HDF5 file was mapped and converted into DAT format, which then underwent automated spike-sorting with KiloSort programme (Pachitariu et al., 2016) in the MatLab environment. Parallelly, the CED-64 file was remapped and filtered with Butterworth band pass filter (fourth order) from 0.3 to 7.5 kHz by a custom-made Spike2 script. Spike-sorting results were merged with the CED-64 files (Spike2 8.11; Cambridge Electronic Design Ltd.) with a custom-written MatLab script. Such prepared files were then inspected manually, and all errors corrected using autocorrelation, crosscorrelation, principal component analysis (PCA) and spike shape inspection.

Data were analysed as firing frequency averaged over 30 s. Cells whose firing rate during the drug application varied from their mean baseline (~10 min) value by at least three standard deviations were pronounced sensitive and included in the analysis of the amplitude of the effect, with an exception of those not active spontaneously. The amplitude of the response was calculated as the maximal value during the response minus the averaged baseline.

2.3.3. Patch clamp

2.3.3.1. Recording.
A brain slice containing the DMH was placed in the recording chamber positioned under an Axioskop 2 FS microscope fitted with infrared differential interference contrast (Göttingen, Germany). The chamber was constantly perfused with carbogenated rACSF, heated to 32 °C. The structure of interest was localised under 5× magnification, after which 40× objective was used to acquire whole-cell configuration. For this, borosilicate glass pipettes (Sutter Instruments, USA; resistance = 4–9 MΩ) filled with an intrapipette solution containing (in mM): 125 potassium gluconate, 20 KCl, 10 HEPES, 2 MgCl2, 4 Na2ATP, 0.4 Na3GTP, 1 EGTA, and 0.05 % biocytin (pH = 7.4, adjusted with 5 M KOH; osmolality 300 mOsmol/kg) and mounted onto an Ag/AgCl electrode were used. Pressure necessary to obtain gigaseal, as well as rupture cellular membrane, was applied with Ez-gSEAL100B Pressure Controller (Neo Biosystem, USA). Recorded signal was amplified by a SC 05LX amplifier (NPI, Germany), low-pass filtered at 3 kHz, digitised at 20 kHz, and visualised using Signal and Spike 2 software (Cambridge Electronic Design Inc., UK).

Patch clamp experiments were performed in voltage clamp mode at −60 mV holding potential. A minimum of 300 s of stable baseline was recorded before Exn4/GLP2/Oxm administration and the recording continued for at least 1000 s after peptide application in order to ensure a complete washout of the drug. Throughout the entire recording, patch clamp stability was monitored by applying a rectangular voltage pulse (duration 1 s, amplitude 35 mV) every 60 s.

2.3.3.2. Immunohistochemical verification.
At the end of the experiment the location of each recorded neuron was verified with immunofluorescence. All brain slices containing a recorded cell were fixed in 4 % PFA in PBS overnight. They were then rinsed in PBS (2 × 10 min) and incubated with 0.6 % Triton-X100 (Sigma-Aldrich, USA) and 10 % normal donkey serum (NDS; Jackson ImmunoResearch, USA) in PBS, for 3 h at room temperature. Primary antibodies solution (72 h at 4 °C) included Cy3-conjugated Extravidin (1:250, Sigma-Aldrich), binding biocytin in the recorded neuron, rabbit neuropeptide Y (NPY) antisera (1:8000, Sigma-Aldrich), used as a marker of the DMH, as well as 0.3 % Triton-X100 and 2 % NDS. After this step, the slices were rinsed in PBS (2 × 10 min) and incubated with secondary, anti-rabbit AlexaFluor 647-conjugated antisera (1:300; Jackson ImmunoResearch) in PBS for 24 h at 4 °C. Finally, the slices were rinsed once more (2 × 10 min), placed onto slides and coverslipped with Fluoroshield™ with DAPI (Sigma-Aldrich).

Immunostained slices were scanned with an epifluorescence microscope (Axio Imager M2, Zeiss). Different subdivisions of the DMH were recognised based on DAPI (smaller, densely packed cells in the cDMH), as well as NPY (dense fibres in both dDMH and vDMH, visibly less dense in cDMH or the neighbouring VMH; Fig. 3A).

2.3.3.3. Data analysis.
From each recording we extracted three 100 s long segments, representative of the cells' postsynaptic activity during the baseline, peptide application, and after the washout of the drug. This enabled us to distinguish between genuine effect of the drug and a continuous drift in PSC generation during the experiment, independent of the tested stimulus. Postsynaptic currents (PSC) were counted in Mini Analysis Software (Synaptosoft, USA). Amplitude of the effect to the drug was calculated as the frequency of PSC during its application minus PSC frequency during the baseline, and compared between daytime/nighttime and dietary groups.

2.3.4. Drugs

Exendin-4 (Exn4; Tocris, UK) glucagon-like peptide 2 (GLP2; Sigma-Aldrich) and oxyntomodulin (Oxm; Tocris) were dissolved in 0.9 % NaCl at 100× concentration, aliquoted, and kept at −20 °C. During the experiment, the stock was diluted in fresh rACSF and applied by bath perfusion. The target concentration of all three drugs was 1 μM.

2.4. Immunofluorescence

2.4.1. Food deprivation (FD) protocol
The food deprivation (FD) protocol was performed on 36 rats (18 fed CD and another 18 fed HFD). After 4 weeks on a diet, the animals were divided into three treatment groups. The first group was an ad libitum-fed control, perfused at ZT14. The further two were food deprived for 48 h (starting and ending at ZT14), after which one of them was perfused straight away (the fasted condition, representing hunger), while the other one was allowed free access to food for the next 2 h (the refeed condition, representing satiety).

All animals were sacrificed between ZT14–17. First, the rats were anaesthetised by isoflurane inhalation (1 ml in the incubation chamber, Baxter) and sodium pentobarbital injection (100 mg/kg body weight, i. p.; Biowet, Poland). After no response to a tail pinch could be observed, transcardial perfusion was performed with PBS followed by 4 % PFA in PBS. Fixed brains were extracted and kept overnight in the same PFA

solution. The next day, 35 μm thick brain slices were cut using a vibroslicer (Leica VT1000S, Germany).

Immunofluorescent labelling started with a 30-min long non-specific site blocking and membrane permeabilization in PBS containing 0.5 % Triton-X100 (Sigma-Aldrich) and 5 % normal donkey serum (NDS, Jackson ImmunoResearch), at room temperature. Then, the slices were incubated with 0.5 % NDS, 0.3 % Triton-X100 and either rabbit anti-cFos antibodies (1:2000, Abcam, UK) or mouse anti-GLP1 antibodies (1:500, Santa Cruz Biotechnology, USA) in PBS for 24 h at 4 °C. After this step, the slices were rinsed in PBS (2 × 10 min) and transferred to a secondary antibodies solution (either AlexaFluor488-conjugated anti-rabbit or Cy3-conjugated anti-mouse antisera; 1:300, Jackson ImmunoResearch) in PBS overnight at 4 °C. After that, the slices were rinsed again (2 × 10 min), mounted onto glass slides and coverslipped with Fluoroshield™ with DAPI (Sigma-Aldrich).

Microphotographs were taken using an epifluorescence microscope (Axio Imager M2, Zeiss, Germany). The compact part of the DMH was recognised with DAPI, as a region of small, densely packed cells, of a characteristic shape. Then, three circular regions of interest (300 px in diameter) were outlined inside each of the DMH subdivisions. Density of the GLP1 fibres was analysed as area fraction (immunoreactive pixels/area) after background subtraction and image binarization via thresholding, averaged over the three measurements.

Cells immunoreactive for cFos were counted manually by a blinded experimenter, separately for each DMH subdivision within a particular slice, and the total area of each part was measured with ZEN 2.5 (blue edition; Zeiss). All cFos-immunoreactive neurons were also DAPI-positive. The analysis was performed on the density of the cFos-positive cells (cell count/area).

2.4.2. Restricted feeding (RF) protocol

The restricted feeding (RF) protocol was performed on 37 rats (18 fed CD and 19 fed HFD). The animals underwent 2 weeks of ad libitum feeding, after which they were fed in a restricted manner (food available between ZT14–20) for the following 2 weeks. Then, they were assigned to one of three groups. The first one was sacrificed 0.5 h before the scheduled meal, the second 1.5 h and the third 3.5 h after the onset of the scheduled meal. The perfusion, the immunofluorescent staining and the microphotograph processing were performed analogically to the procedure described in *2.4.1. Food deprivation protocol*, with the only differences being the concentration of the primary anti-GLP1 antibody (1:400) and both secondary antibodies (1:400).

2.5. Statistical analysis

Statistical analysis was performed in R (Version 4.0.4; Team, 2021) and RStudio (Version 1.4.1106, PBC; Team, 2015). Frequency of the response to the applied peptides was analysed with binomial regression (a generalised linear mixed effects model with a binomial response value), whereas for continuous outcome variables general linear models were fitted. To account for multiple observations from the same animal and/or brain slice a random effect was included in a mixed model (random intercepts for nested designs and random slopes for repeated measures). Mixed models were fitted with *lme4* and *lmerTest* packages (Bates et al., 2015; Kunzetsova et al., 2017) and analysed with type III ANOVA (with Satterthwaite's method for the degrees of freedom estimation). Outliers were detected with Bonferroni test from *car* package (Fox and Weisberg, 2019), detecting mean-shifting (influential) data points within the model. Post hoc analyses were performed using *emmeans* package (Lenth, 2021), and *p*-value corrected for multiple comparisons with Tukey method. Assumptions of a general linear model were checked with Shapiro-Wilk normality test from *rstatix* package (Kassambara, 2021) and Levene test for homoscedasticity from *car* package, normality of the residuals' distribution was analysed with QQ-plots (*ggpubr*; Kassambara, 2020). In the case of not meeting the normality or homogeneity assumptions the values were transformed

either using odd roots (MEA and patch clamp – response amplitude: both positive and negative values) or Box-Cox (BC) transformation (for immunofluorescence – only positive values; package: *MASS*; Venables and Ripley, 2002), defined as: $BC(y) = (y^\lambda - 1)/\lambda$, where λ is a value that provides the best approximation for the normal distribution of the response variable (Box and Cox, 1964). Detailed results from all the models are presented in Tables S1 (ANOVA results of the generalised linear models), S2 (ANOVA results of the general linear models), S3 (results of the multiple comparisons) and S4 (mean, SD and n values).

3. Results

3.1. Localisation of Glp1r and Glp2r mRNA in the DMH

Our study on the high-fat diet-evoked changes in the PPG signalling within the DMH started with a confirmation of *Glp1r* and *Glp2r* expression in the structure as well as its precise localisation using in situ hybridisation. In line with previous reports (Merchenthaler et al., 1999; Tang-Christensen et al., 2000, 2001; Cork et al., 2015; Lee et al., 2018; Maejima et al., 2021; Huang et al., 2022), we observed fluorescent signal from both *Glp1r*- and *Glp2r*-targeting probes within the DMH. Moreover, the two types of receptors appeared to occupy distinct subdivisions of the DMH, with little if any overlap or colocalization (Fig. 1A). *Glp1r* expression was restricted to individual cells within vDMH and dDMH, densely filled with the fluorescent probe. The analysis of the density of the *Glp1r*-positive cells confirmed the observed distribution ($F_{2,26}$ = 80.06, $p < 0.0001$, $n = 36$), showing the highest abundance per area in the dDMH (dDMH vs vDMH: $t_{20} = 5.28$, $p = 0.0001$; dDMH vs cDMH: t_{20} = 12.6, p < 0.0001), followed by vDMH (vDMH vs cDMH: $t_{20} = 7.32$, p < 0.0001). No differences between the dietary groups were observed in any DMH subdivision (diet: $F_{1,4} = 0.009$, $p = 0.93$; diet × DMH div.: $F_{2,26} = 0.79$, $p = 0.46$, $n = 36$, Fig. 1B).

The intensity of *Glp1r* expression was analysed as the density of the fluorescent signal. Here, also differences within the DMH were spotted, with no dietary influence (diet: $F_{1,4} = 0.1$, $p = 0.76$; DMH div.: $F_{2,22}$ = 21.98, $p < 0.0001$; diet × DMH div.: $F_{2,22} = 0.0061$, $p = 0.99$, $n = 39$). Interestingly, in this case vDMH and dDMH showed the same level of *Glp1r* expression ($t_{22} = 1.63$, $p = 0.25$), again higher than in the cDMH (vDMH vs cDMH: $t_{22} = 4.75$, $p = 0.0003$; dDMH vs cDMH: $t_{22} = 6.83$, $p < 0.0001$; Fig. 1C).

On the other hand, *Glp2r* mRNA was present predominantly in the cDMH ($F_{2,22} = 30.41$, p < 0.0001, n = 39; cDMH vs vDMH: $t_{22} = 7.31$, p < 0.0001; cDMH vs. dDMH: $t_{22} = 6.00$, p < 0.0001), with equally little *Glp2r* expressed in the other two subdivisions ($t_{22} = 1.31$, $p = 0.4$; Fig. 1C). Its expression appeared diffused across the entire cDMH area, which together with compactly packed neurons did not allow for a distinction of individual, *Glp2r*-positive cells.

3.2. Exn4/Oxm/GLP2 impact on the DMH neuronal firing

Despite extensive data on the presence of the GLP1 and GLP2 receptors in the DMH (Merchenthaler et al., 1999, Tang-Christensen et al., 2000, 2001, Cork et al., 2015, Lee et al., 2018, Maejima et al., 2021, Huang et al., 2022), their ability to induct cFos expression in the DMH (Tang-Christensen et al., 2000; Maejima et al., 2021; Huang et al., 2022), as well as the DMH-mediated influence of the PPG-derived peptides on the animals feeding behaviour (Maejima et al., 2021), our knowledge of their impact on the DMH electrophysiology is limited. Therefore, we performed a set of multi-electrode array (MEA) experiments on brain slices acquired from animals fed either CD or HFD, both during the day and at night (factor - LD).

All three tested peptides (Exn4, GLP2 and Oxm) were shown to impact the electrical activity of the DMH neurons, predominantly causing an increase in their firing rate. Although these receptors had been shown to localise in very specific parts of the structure, neurons responsive to the applied substances were spotted all over the structure,
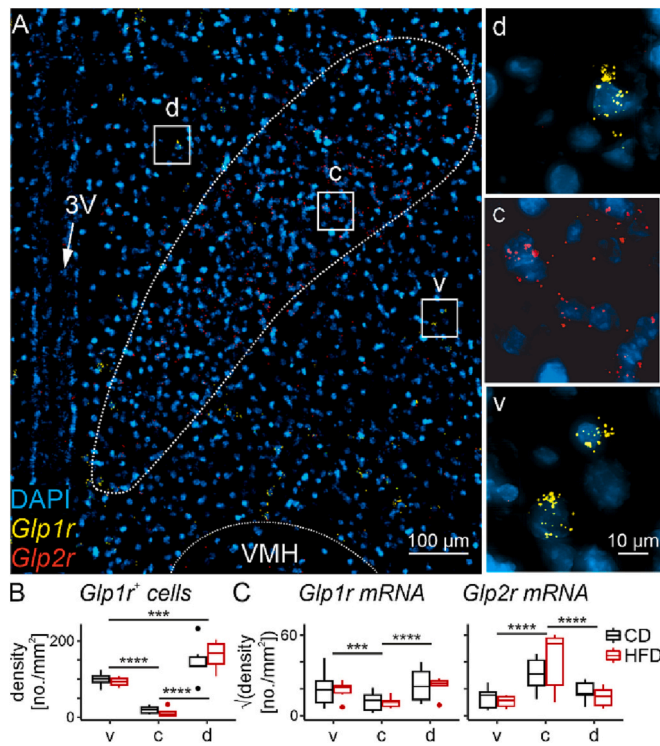
Fig. 1. *Localisation of Glp1r and Glp2r mRNA in the DMH*

A. Representative microphotograph of a brain slice acquired from a HFD-fed rat, tagged with probes for glucagon-like peptide 1 receptor (*Glp1r*) and glucagon-like peptide 2 receptor (*Glp2r*), together with DAPI staining, indicating the location of the compact part of the DMH (c) as the region of densely packed cells. Each of the DMH subdivisions was additionally zoomed-in, in order to better visualise the specific distribution of both signals, with *Glp1r* being restricted to the ventral (v) and dorsal (d) parts of the structure, and *Glp2r* mostly present in the cDMH. 3 V – third ventricle, VMH – Ventromedial Hypothalamus.

B. Graphs presenting the results from the analysis of the density of *Glp1r*-positive cells (diet: $F_{1,4} = 0.009$, $p = 0.93$; DMH div.: $F_{2,26} = 80.06$, $p < 0.0001$; diet × DMH div.: $F_{2,26} = 0.79$, $p = 0.46$, $n = 36$).

C. Graphs presenting the results from the analysis of the density of *Glp1r* (diet: $F_{1,4} = 0.1$, $p = 0.76$; DMH div.: $F_{2,22} = 21.98$, $p < 0.0001$; diet × DMH div.: $F_{2,22} = 0.0061$, $p = 0.99$, $n = 39$) and *Glp2r* mRNA (diet: $F_{1,4} = 0.015$, $p = 0.91$; DMH div.: $F_{2,22} = 30.41$, $p < 0.0001$; diet × DMH div.: $F_{2,22} = 2.93$, $p = 0.074$, $n = 39$). ***$p < 0.001$, ****$p < 0.0001$. Box-and-whisker plots present the median value, the interquartile range (IQR; box) and the minimum-to-maximum range of values, not exceeding 1.5 * IQR (whiskers). Data points outside this range are plotted individually.

with no clear spatial pattern in the magnitude of the effect either (Fig. 2A, E, I). The percentage of cells responsive to GLP2 and Oxm did not differ between the experimental groups (GLP2: CD daytime - 34.48 %, CD nighttime - 52.63 %, HFD daytime - 35.46 %, HFD nighttime - 44.68 %; diet: $\chi_1^2 = 0.0051$, $p = 0.94$; LD: $\chi_1^2 = 2.98$, $p = 0.085$, diet × LD: $\chi_1^2 = 0.15$, $p = 0.7$, $n = 352$; Oxm: CD daytime: 50 %, CD nighttime: 38.46 %, HFD daytime: 44.79 %, HFD nighttime: 44.74 %%; diet: $\chi_1^2 = 0.19$, $p = 0.67$; LD: $\chi_1^2 = 1.4$, $p = 0.24$, diet × LD: $\chi_1^2 = 1.09$, $p = 0.3$, $n = 363$), however the sensitivity to Exn4 was increased under HFD (CD daytime: 42.86 %, CD nighttime: 46 %, HFD daytime: 65.05 %, HFD nighttime: 50 %; diet: $\chi_1^2 = 7.68$, $p = 0.0056$; LD: $\chi_1^2 = 0.11$, $p = 0.74$, diet × LD: $\chi_1^2 = 2.46$, $p = 0.12$, $n = 316$). Moreover, when comparing the types of responses (increase vs. decrease in firing rate) we noticed a higher percentage of cells lowering their frequency of action potential generation at night than during the day, for all three peptides (Exn4: diet: $\chi_1^2 = 1.14$, $p = 0.29$; LD: $\chi_1^2 = 5.08$, $p = 0.024$, $n = 167$; Oxm: diet: $\chi_1^2 = 1.11$, p = 0.29; LD: $\chi_1^2 = 4.33$, $p = 0.037$, $n = 163$; GLP2: diet: $\chi_1^2 = 0.3$, $p = 0.59$; LD: $\chi_1^2 = 4.69$, p = 0.03, $n = 143$; Fig. 2D, H, L). Nevertheless,

those cells constituted a vast minority, and their total number did not allow for statistical comparison of the amplitude of the effect between the groups. We also excluded cells which were completely silent during baseline recording ($n = 8$; total for all peptides), as their response could be highly dependent on the magnitude of hyperpolarisation below the threshold for action potential generation.

We have previously shown that HFD-feeding increases spontaneous activity in the DMH during the day (Sanetra et al., 2022b). Baseline firing rate might alone be an important factor influencing the magnitude of a response to a drug, therefore we have added it to the model as a covariate, and run an ANCOVA to find out whether there are any differences in the relationship between neuronal spontaneous activity and the amplitude of the response to Exn4/GLP2/Oxm between our dietary/LD groups.

Taking into account all predictors in the model, HFD was shown to reduce the amplitude of the response to both Exn4 ($F_{1,73} = 4.78$, $p = 0.032$, $n = 122$) and Oxm ($F_{1,77} = 7.91$, $p = 0.0062$, $n = 130$). However, a strong correlation with baseline activity was also observed (Exn4: $F_{1,106} = 9.04$, $p = 0.0033$, n = 122; Oxm: $F_{1,122} = 11.78$, $p = 0.00082$, n = 130), as well as an interaction between the diet and the baseline activity (Exn4: $F_{1,106} = 6.05$, $p = 0.016$, $n = 122$; Oxm: $F_{1,122} = 6.31$, $p = 0.013$, n = 130; Fig. 2B-C, 2F-G), indicating that the link between cells' spontaneous and evoked activity becomes disrupted under HFD. In the case of GLP2, only an effect of baseline firing rate was significant ($F_{1,107} = 10.69$, $p = 0.0015$, $n = 115$), with no changes between the dietary groups ($F_{1,107} = 0.0052$, $p = 0.94$, n = 115; Fig. 2J-K).

These results provide an insight into HFD-mediated changes in DMH neurons' sensitivity to Exn4 and Oxm, and negate HFD influence on the responsiveness to GLP2.

3.3. Exn4/Oxm/GLP2 impact on the synaptic network in the DMH

Lack of a specific spatial distribution in the responsiveness to the PPG-derived peptides contrasting a clear separation in the receptor expression led us to hypothesise that observed effects may attribute to a mix of postsynaptic and network-driven actions of PPGs. In order to confirm such phenomenon, we performed a patch-clamp study in voltage clamp mode, and analysed changes in the frequency of the postsynaptic currents (PSC) due to the drug application between our diet/LD groups. Thanks to the post-recording immunostaining, we were able to pinpoint the exact location on the recorded cell (DMH division: dDMH, cDMH or vDMH; Fig. 3A) and add it to the model as a covariate, however in no case was it statistically significant (Exn4: $F_{2,43} = 2.78$, $p = 0.073$, $n = 57$; Oxm: $F_{2,43} = 1.45$, $p = 0.25$, $n = 49$; GLP2: $F_{2,36} = 0.33$, $p = 0.72$, $n = 43$).

Various responses were spotted after Exn4/Oxm/GLP2 bath application, including both an increase (Fig. 3B) and a decrease in PSC frequency, as well as no effect. The response to GLP2 was shown to depend only on the time of day ($F_{1,26} = 10.14$, $p = 0.0038$, n = 43) with higher values during daytime regardless of the diet fed ($F_{1,26} = 0.33$, $p = 0.57$, n = 43), whereas the responsiveness to Exn4 was also influenced by the diet (diet × LD: $F_{1,22} = 5.01$, $p = 0.036$, n = 57). HFD group presented a higher response amplitude than the CD during the day ($t_{24} = 2.08$, $p = 0.048$), which caused a strong day/night difference in this group ($t_{27} = 3.73$, $p = 0.0009$). Contrary to the results obtained with the MEA, the PSC frequency response to Oxm did not follow the pattern observed for Exn4, as no changes were spotted between any of the groups (LD: $F_{1,25} = 0.96$, $p = 0.34$, diet: $F_{1,25} = 3.76$, $p = 0.064$, LD × diet: $F_{1,25} = 0.59$, $p = 0.45$, $n = 49$; Fig. 3C).

These data confirm the synaptic mediation of Exn4 and GLP2 effects, which could be happening either directly by activating presynaptic receptors or via postsynaptic response. Either way, the cue of the PPG-derived peptides, despite locally distributed receptors, appears to get spread out throughout the entire structure due to the synaptic network. On top of that, our results suggest that this process varies between day and night for both Exn4 and GLP2, and changes under HFD for Exn4, but
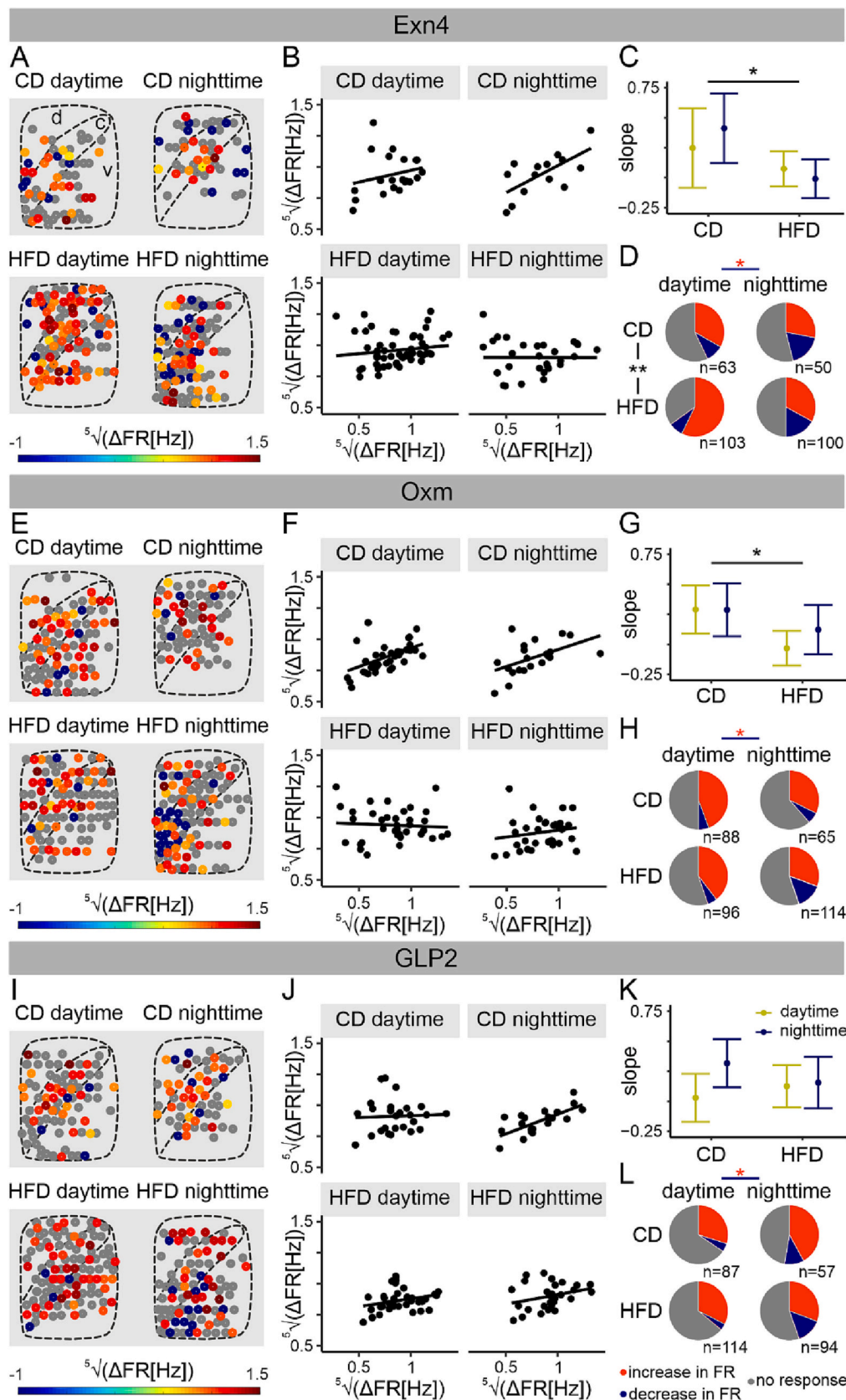
Fig. 2. *Exn4/Oxm/GLP2 impact on the DMH neuronal firing*

A, E, I. Spatial distribution of the cells sensitive to Exn4 (A)/Oxm (E)/GLP2 (I) together with colour-coded amplitude of the response to the tested peptides. Grey colour indicates non-responsive neurons. DMH subdivisions are indicated as: c – compact, d – dorsal, v – ventral.

B - C, F - G, J - K. Correlation of the amplitude of the excitatory response to Exn4 (B)/Oxm (F)/GLP2 (J) and the baseline activity for each of the diet/LD groups. Analysis of the regression slopes revealed differences between the diets for Exn4 ($F_{1,106} = 6.05$, $p = 0.016$, $n = 122$; C) and Oxm ($F_{1,122} = 6.31$, $p = 0.013$, $n = 130$; G), but not for GLP2 ($F_{1,107} = 0.11$, $p = 0.74$, $n = 115$; K). Slope values presented as estimate ± 95 % CI.

D, H, L. Pie charts representing proportions of cells sensitive to Exn4 (D)/Oxm (H)/GLP2 (L), as well as responding with increase and decrease in firing rate (FR). Higher number of neurons was sensitive to Exn4 in the HFD group compared to CD ($\chi^2_1 = 7.68$, $p = 0.0056$, $n = 316$). For each peptide, the percentage of cells responding with a decrease in FR was higher at night than during the day (Exn4: $\chi^2_1 = 5.08$, $p = 0.024$, $n = 167$, Oxm: $\chi^2_1 = 4.33$, $p = 0.037$, $n = 163$, GLP2: $\chi^2_1 = 4.69$, $p = 0.03$). Black asterisks indicate differences in the total number of responsive cells, whereas red ones present the results of the analysis comparing cells responding in different ways within the sensitive population. CD – control diet, Exn4 – exendin-4, GLP2 – glucagon-like peptide 2, HFD – high-fat diet, Oxm – oxyntomodulin. *$p < 0.05$, **$p < 0.01$.
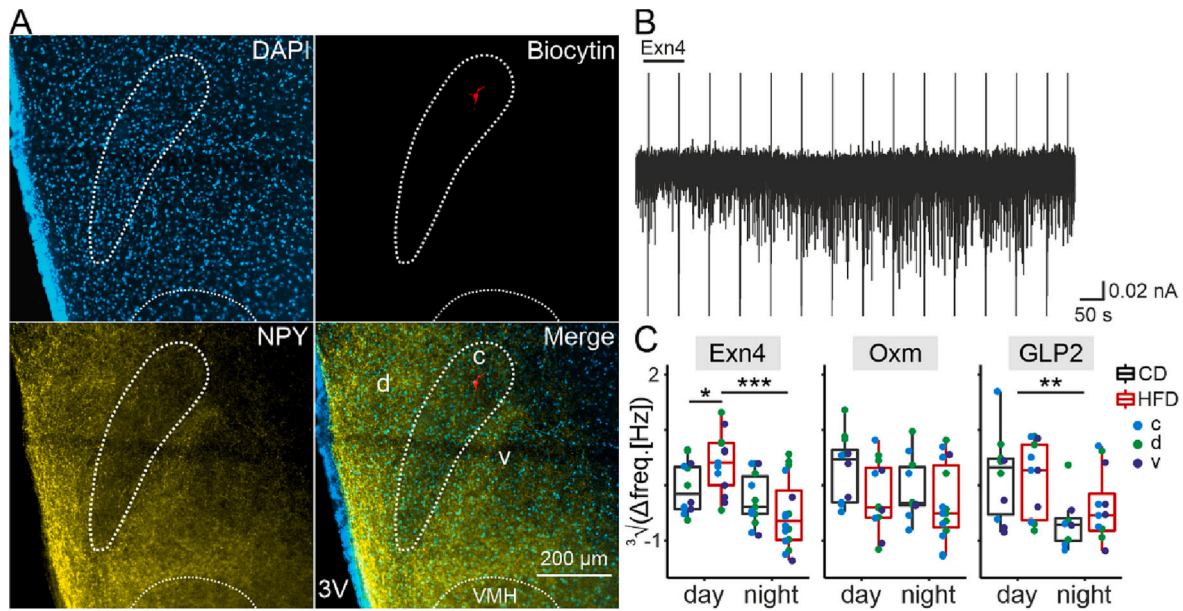
Fig. 3. *Exn4/Oxm/GLP2 impact on the synaptic network in the DMH*

A. Representative microphotographs presenting a post-recording immunostained brain slice. The recorded neuron is visible due to biocytin presence inside the intrapipette solution. DAPI, and well as neuropeptide Y (NPY) were used to outline the different subdivisions of the DMH: the compact (c) part, recognised as densely packed cells with little NPY immunoreactivity, separating the structure into dorsal (d) and ventral (v) parts. 3 V – third ventricle, VMH – Ventromedial Hypothalamus.

B. Representative recording showing a transient increase in post-synaptic currents (PSC) after exendin-4 (Exn4) application.

C. Comparison of the PSC frequency (freq.) between dietary (control – CD vs high-fat diet – HFD) and LD (day/night) groups for each of the investigated peptides: Exn4 (diet: $F_{1,21} = 0.76$, $p = 0.39$; LD: $F_{1,22} = 9.79$, $p = 0.0048$, DMH div.: $F_{2,43} = 2.78$, $p = 0.073$; diet × LD: $F_{1,22} = 5.01$, $p = 0.036$, $n = 57$; day: $t_{24} = 2.08$, $p = 0.048$, HFD: $t_{27} = 3.73$, $p = 0.0009$), Oxm (LD: $F_{1,25} = 0.96$, $p = 0.34$, diet: $F_{1,25} = 3.76$, $p = 0.064$, DMH div.: $F_{2,43} = 1.45$, $p = 0.25$, LD × diet: $F_{1,25} = 0.59$, $p = 0.45$, $n = 49$) and GLP2 (LD: $F_{1,26} = 10.14$, $p = 0.0038$, diet: $F_{1,26} = 0.33$, $p = 0.57$, DMH div.: $F_{2,36} = 0.33$, $p = 0.72$, LD × diet: $F_{1,26} = 0.73$, $p = 0.4$, $n = 43$). *$p < 0.05$, **$p < 0.01$, ***$p < 0.001$. Box-and-whisker plots present the median value, the interquartile range (IQR; box) and the minimum-to-maximum range of values, not exceeding 1.5 * IQR (whiskers). Data points are colour coded to visualise the lack of differences between DMH subdivisions.

not Oxm, also signalising differences between the mechanisms underlying the action of these two peptides.

3.4. Density and distribution of GLP1-immunoreactive fibres and cFos-positive cells in the DMH under different metabolic states

Potential changes in PPG signalling could be occurring on two distinct levels: sensitivity of the DMH neurons to these peptides, and/or the amount of the peptides released. Therefore, after observing differences in the responsiveness of the DMH cells between the diets, we decided to investigate the density of GLP1-positive neuronal fibres, as a representative of the amount of the co-released peptides present in the structure. Keeping in mind, that PPG-derived peptides are involved in satiety signalling, and their production as well as release might depend on the animals' metabolic states, we performed the immunofluorescence staining under three different conditions for each dietary group. The first group was an ad libitum-fed control, the second was food-deprived for 48 h (hunger state), and the third one was also food-deprived for 48 h, but then refed for 2 h (satiety state).

In order to confirm a lack of difference in body weight after 4 weeks on a diet the animals were weighed once a week, starting at week 0 (the onset of the experiment). As previously (Chrobok et al., 2022; Sanetra et al., 2022b), we observed time-related increase in the weight of the rats ($F_{4,34} = 1636.53$, $p < 0.0001$, $n = 36$) and an interaction between the diet and the week ($F_{4,34} = 8.34$, $p < 0.0001$, $n = 36$), but no significant effect of HFD feeding at any time point ($F_{1,34} = 0.022$, $p = 0.88$, $n = 36$; week 4: $t_{34} = -0.73$, $p = 0.47$; Fig. 4B). The adequacy of the experimental protocol was verified by analysing stomach mass after cull. Food-deprived group (FD) had significantly lighter stomachs than either the ad libitum (AL, $F_{2,30} = 255.83$, $p < 0.0001$, $n = 36$, $t_{30} = -7.68$, $p < 0.0001$), or refed groups ($t_{30} = -22.27$, $p < 0.0001$), and the latter one

was also heavier than the control group ($t_{30} = 14.59$, $p < 0.0001$). On top of that, stomachs obtained from HFD-fed animals were lighter than the CD group ($F_{1,30} = 6.45$, $p = 0.017$, $n = 36$; Fig. 4C), also in line with our previous reports of decreased food intake (total food mass) in these rats (Chrobok et al., 2022, Sanetra et al., 2022b).

As documented by Renner et al. (2012), vast majority of the GLP1-positive fibres occupied the ventral subdivision of the DMH, with some present in the dorsal part, and very little in *pars compacta* ($F_{2,112} = 129.23$, $p < 0.0001$, $n = 186$). However, an interaction with the diet was also noted ($F_{2,112} = 3.46$, $p = 0.035$, $n = 186$), suggesting different susceptibility of the three substructures to HFD. Furthermore, a significant interaction between diet and treatment (metabolic state) indicated changes in the dependence of the GLP1-immunoreactivity on the satiety state between the dietary groups ($F_{2,28} = 3.74$, $p = 0.036$, $n = 186$). Indeed, the GLP1 fibre density was greater after the refeed than during food deprivation in both dDMH ($t_{72} = 2.84$, $p = 0.016$) and vDMH ($t_{72} = 2.95$, $p = 0.012$) and also during ad libitum feeding in vDMH ($t_{66} = 2.83$, $p = 0.017$), but only for CD-fed rats. HFD completely abolished the observed phenomenon. In dDMH this happened due to an increased GLP1-immunoreactivity during food deprivation ($t_{72} = 2.62$, $p = 0.011$), whereas in the vDMH, fibre density during the refeed appeared near-to-significantly lower than for the control diet ($t_{62} = -1.94$, $p = 0.057$; Fig. 4A, D). All back-transformed mean + 95 % CI values for each group can be found in Table S4.

DMH has been shown to respond to satiety with an intense cFos expression, predominantly in cells located in close proximity to the GLP1-immunoreactive fibres (Renner et al., 2012; Huang et al., 2022). The study by Renner et al. (2012) also showed that this cFos expression is partially mediated by the GLP1-positive NTS neurons sending projections to the DMH. Therefore, we also analysed the density of cFos-positive cells in the same conditions as done for GLP1
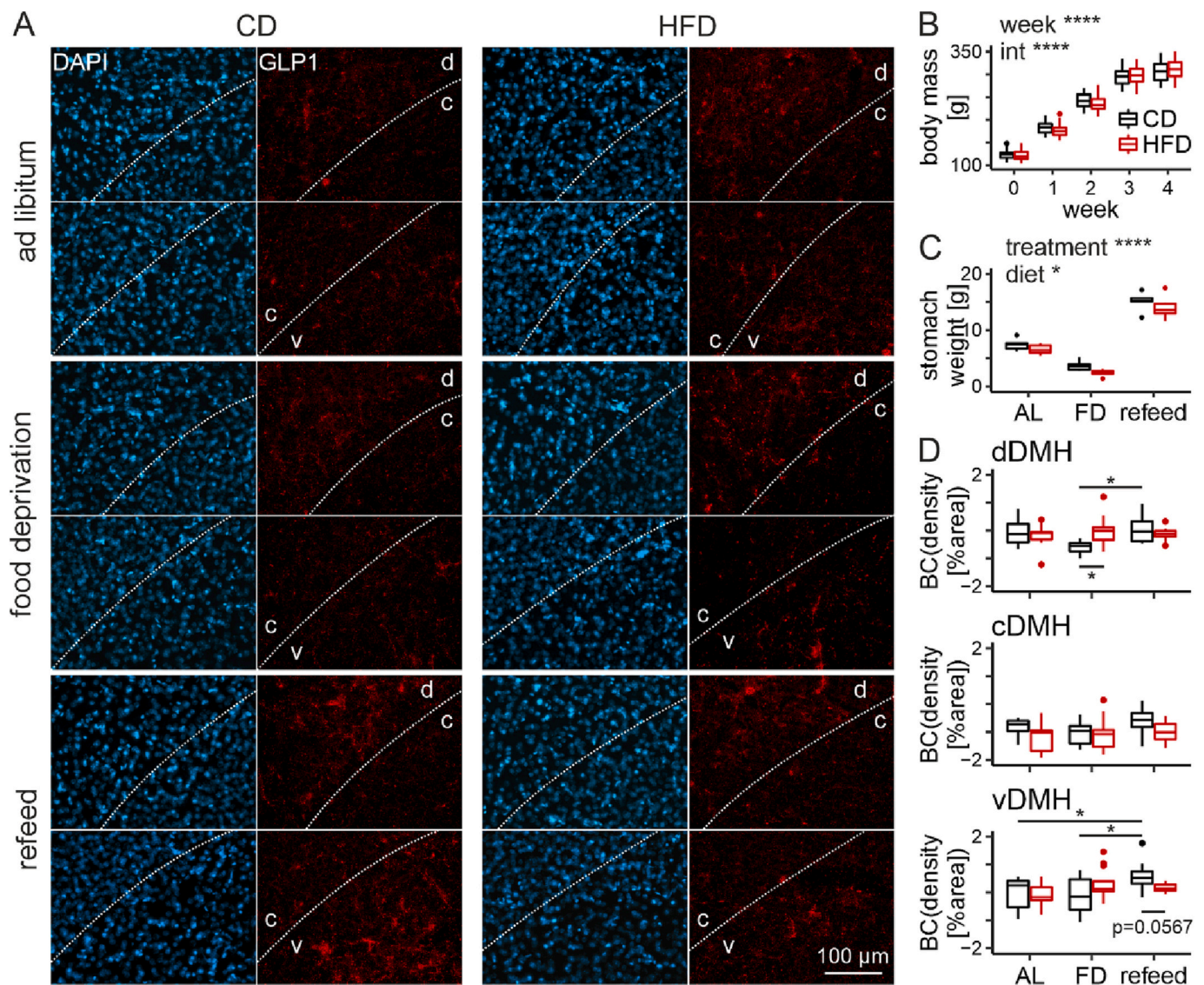
Fig. 4. *GLP1-immunoreactive fibre density in the DMH under different metabolic states*

A. Representative microphotographs visualising GLP1-positive fibres in different parts of the DMH. The highest density was observed in the ventral part of the structure (v), followed by the dorsal part (d) and the lowest in the compact part (c; $F_{2,112} = 129.23$, $p < 0.0001$, $n = 186$).

B. Comparison of body mass for control (CD) and high-fat diet (HFD)-fed rats across the 4 weeks of the experiment (week: $F_{4,34} = 1636.53$, $p < 0.0001$; diet: $F_{1,34} = 0.022$, $p = 0.88$; week × diet: $F_{4,34} = 8.34$, $p < 0.0001$, $n = 36$).

C. Comparison of the stomach weight at the end of the experimental procedure (treatment: $F_{2,30} = 255.83$, $p < 0.0001$; diet: $F_{1,30} = 6.45$, $p = 0.017$; treatment × diet: $F_{2,30} = 0.084$, $p = 0.92$, n = 36).

D. Comparison of the GLP1 immunoreactivity between dietary/treatment groups for each of the DMH subdivisions (diet: $F_{1,28} = 0.4$, $p = 0.53$; treatment: $F_{2,28} = 3.17$, $p = 0.058$; DMH div.: $F_{2,112} = 129.23$, $p < 0.0001$; diet × treatment: $F_{2,28} = 3.74$, $p = 0.036$; diet × DMH div.: $F_{2,112} = 3.46$, $p = 0.035$; treatment × DMH div.: $F_{4,112} = 1.41$ $p = 0.24$; diet × treatment × DMH: $F_{4,112} = 0.83$, $p = 0.51$; $n = 186$). BC—Box–Cox transformed values ($\lambda = 0.1414$), AL – ad libitum, FD – food deprivation, $*p < 0.05$, $****p < 0.0001$. Box-and-whisker plots present the median value, the interquartile range (IQR; box) and the minimum-to-maximum range of values, not exceeding 1.5 * IQR (whiskers). Data points outside this range are plotted individually.

immunoreactivity, to see whether HFD-related changes in GLP density translate onto cellular activity of the DMH neurons.

Similarly to the results from the analysis of the GLP1-immunoreactivity, the density of cFos positive cells in the vDMH was also higher after the refeed comparing to either FD or AL groups ($F_{2,29} = 13.86$, $p < 0.0001$, $n = 204$; CD FD vs refeed: $t_{46} = -4.07$, $p = 0.0005$; AL vs refeed: $t_{50} = -3.23$, $p = 0.0062$), however in the case of cFos this effect was also present for the HFD-fed rats (FD vs refeed: $t_{46} = -4.95$, p < 0.0001; AL vs refeed: $t_{48} = -3.4$, $p = 0.0039$). Interestingly, a difference between the diets was observed in the density of cFos-positive cells after refeeding in the cDMH ($t_{41} = -2.87$, $p = 0.0064$), with higher numbers under HFD, which caused cFos density to vary between

FD and refeed conditions also in this part of the structure ($t_{46} = -4.8$, $p = 0.0001$; Fig. 5). Same as for GLP1 immunoreactivity, generally the highest density of cFos-positive cells was observed in the vDMH, and the lowest in the cDMH ($F_{2,124} = 154.85$, $p < 0.0001$, n = 204), which was most apparent for the refed groups (Fig. 5A).

These results show that although HFD disrupts GLP1 satiety signalling in relation to the amount of peptide present in the structure, the cellular response to a refeed condition in the form of cFos expression remains mostly unchanged, possibly due to the abundance of other signalling molecules, or various compensatory mechanisms.
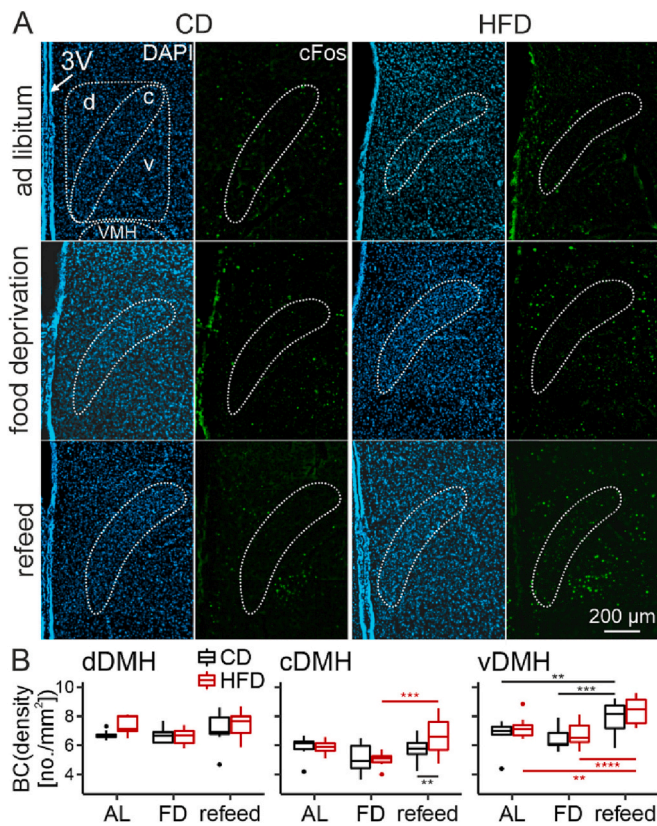
Fig. 5. *Density and distribution of cFos-positive cells in the DMH under different metabolic states*

A. Representative microphotographs presenting brain slices acquired from each dietary (CD – control diet, HFD – high-fat diet) and treatment group (AL – ad libitum, FD – food deprivation, and refeed). 3 V – third ventricle, VMH – Ventromedial Hypothalamus.

B. Graphs presenting the results from the analysis performed for each DMH subdivision separately (c – compact, d – dorsal, v – ventral; diet: $F_{2,29} = 2.87$, $p = 0.1$; treatment: $F_{2,29} = 13.86$, $p < 0.0001$; DMH div.: $F_{2,124} = 154.85$, $p < 0.0001$; diet × treatment: $F_{2,29} = 0.66$, $p = 0.53$; diet × DMH div.: $F_{2,124} = 0.21$, $p = 0.81$; treatment × DMH div.: $F_{4,124} = 7.98$, $p < 0.0001$; diet × treatment × DMH: $F_{4,124} = 2.88$, $p = 0.026$; $n = 204$). BC—Box–Cox transformed values ($\lambda = 0.1010$). $**p < 0.01$, $***p < 0.001$, $****p < 0.0001$. Box-and-whisker plots present the median value, the interquartile range (IQR; box) and the minimum-to-maximum range of values, not exceeding 1.5 * IQR (whiskers). Data points outside this range are plotted individually.

3.5. Density and distribution of GLP1-immunoreactive fibres and cFos-positive cells in the DMH under restricted feeding (RF)

The DMH is well known for its susceptibility to time-restricted feeding, influencing clock gene expression (Mieda et al., 2006; Verwey et al., 2007, 2008, 2009; Minana-Solis et al., 2009), cFos immunoreactivity (Gooley et al., 2006; Verwey et al., 2007) and electrical activity (Sanetra et al., 2022b) within the structure. Thus, we repeated our immunofluorescent staining on animals which had been fed in a restricted manner. For this we used 37 rats (18 fed CD and 19 fed HFD), which were initially fed ad libitum (first 2 weeks), and then for the next 2 weeks were allowed unlimited access to food but only between ZT14–20. At the end of the protocol animals were perfused either half an hour before (time point −0.5 h), 1.5 h or 3.5 h after the onset of the scheduled meal.

Consistently with the FD protocol the rats were weighed every week (for the duration of the RF protocol – weeks 2–4), and again despite a significant interaction between diet and week ($F_{2,28} = 4.13$, $p = 0.027$, $n = 37$; Fig. 6A) the HFD-fed group did not become heavier than the control during the experiment (week 4: $t_{35} = 0.9$, $p = 0.37$). Here, we

also weighed the food provided, and left after the meal in order to calculate the amount eaten during the 6 h window. Similarly to the data presented before (Chrobok et al., 2022; Sanetra et al., 2022b), HFD-fed animals were shown to eat fewer grams ($F_{1,35} = 104.8$, $p < 0.0001$, $n = 37$), but more calories per kilogram of body mass ($F_{1,35} = 56.64$, p < 0.0001, n = 37), however in the second case, this effect was only temporary, and disappeared completely by the end of the 4th week ($t_{35} = 1.3$, $p = 0.2$; Fig. 6A). Surprisingly, and unlike previously, the stomachs of HFD-fed animals were not lighter than the control group ($F_{1,31} = 0.035$, $p = 0.85$, n = 37), only differences between conditions (time before/after the meal onset) were spotted ($F_{2,31} = 139.24$, $p < 0.0001$, n = 37; Fig. 6A).

Also contrary to the FD protocol, the density of GLP1-positive neuronal fibres remained unaltered by the anticipated metabolic state ($F_{2,25} = 0.054$, $p = 0.95$, $n = 234$), neither did it depend on the diet ($F_{1,25} = 0.42$, $p = 0.52$, n = 234). The only significant factor here was the DMH division ($F_{2,144} = 146.05$, p < 0.0001, n = 234), which unsurprisingly showed the same pattern as in the previous experiment – majority of the GLP1 fibres located in the vDMH, and the lowest density in the cDMH (Fig. 6B-C).

The same spatial distribution was observed for the density of cFos-positive cells ($F_{2,170} = 104.37$, p < 0.0001, $n = 273$). On the other hand, cFos-immunoreactivity, unlike the GLP1 density, varied depending on the perfusion time in relation to meal onset ($F_{2,28} = 21.7$, p < 0.0001, n = 273). Although the effect of the diet was not significant ($F_{1,28} = 0.067$, $p = 0.8$, n = 273), we observed an interaction between diet and DMH division ($F_{2,170} = 5.78$, $p = 0.0037$, n = 273), as well as between the DMH division and the time of cull ($F_{4,170} = 3.96$, $p = 0.0042$, n = 273; Fig. 6D-E). For each structure and both diets the lowest density of cFos-positive cells was recorded before the scheduled meal, comparing to both time points after the onset of the meal. The only difference between the diets regarded the density of cFos-immunoreactive cells 1.5 h after meal onset in the vDMH, being lower under HFD ($t_{33} = -2.15$, $p = 0.039$; Fig. 6D-E). All cFos-immunoreactive cells colocalised with DAPI (Fig. 6F).

The results presented in this section indicate differences in both GLP1 and cFos immunoreactivity in response to hunger and satiety depending on their predictability. Moreover, the susceptibility to HFD also appears to change when these metabolic states had been anticipated.

4. Discussion

The presented study investigated PPG signalling in the DMH, together with its HFD-induced alterations, on multiple levels from the distribution of the receptors, through the peptide amount in different conditions, up to the neuronal sensitivity.

4.1. GLP1 and GLP2 receptor and GLP1 fibre spatial distribution

First, in situ hybridisation was used to confirm a very specific spatial pattern of the *Glp1r* and *Glp2r* mRNA for both diets. As observed by others (Merchenthaler et al., 1999; Tang-Christensen et al., 2000, 2001; Cork et al., 2015; Lee et al., 2018; Maejima et al., 2021), both receptors were found by us to be expressed within the DMH, with GLP2R present almost exclusively within the cDMH (Tang-Christensen et al., 2000, 2001), and GLP1R mostly outside of it (Renner et al., 2012), although in the second case there are inconsistencies between studies, with some showing a more even coverage of the *Glp1r*-expressing cells across the structure (Cork et al., 2015; Maejima et al., 2021). Differences could stem from species-specificity (mouse vs. rat), or probe sensitivity, failing to detect the signal in some cells. Even though the signal acquired appeared very intense and dense in the neurons where it was spotted, there is a possibility of much lower expression in other cells, resulting in a barely detectable signal, which would not have been counted as a *Glp1r*-expressing cell. For this reason, as well as to investigate the level
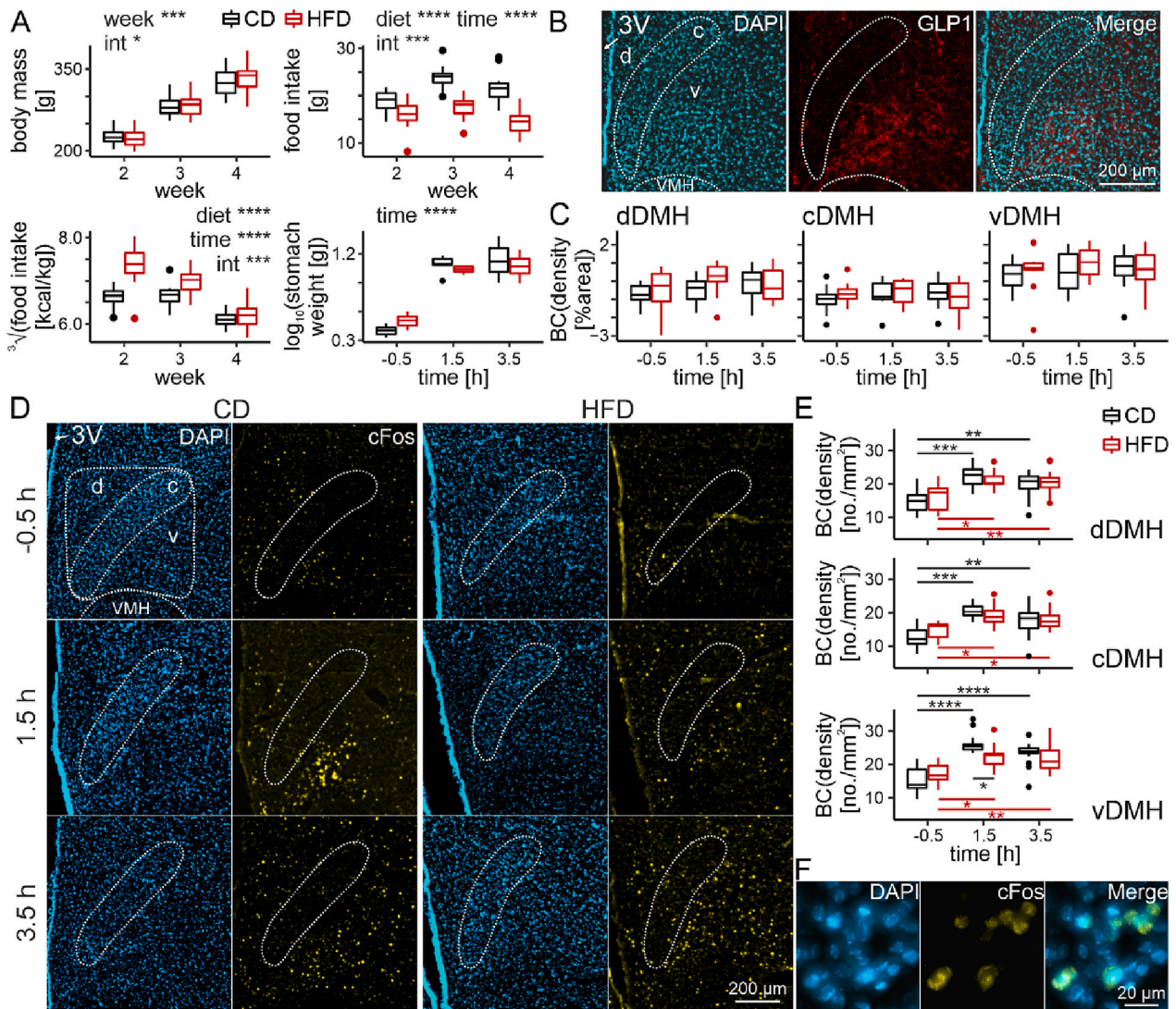
Fig. 6. *Density and distribution of GLP1-immunoreactive fibres and cFos-positive cells in the DMH under restricted feeding (RF)*

A. Graphs presenting body weight (week: $F_{2,28} = 1485.61$, $p < 0.0001$; diet: $F_{1,35} = 0.098$, $p = 0.76$; week × diet: $F_{2,28} = 4.13$, $p = 0.027$, $n = 37$), total meal size in grams (week: $F_{2,35} = 30.96$, p < 0.0001; diet: $F_{1,35} = 104.8$, p < 0.0001; week × diet: $F_{2,35} = 11.64$, $p = 0.00013$, $n = 37$) and in kcal/kg body weight (week: $F_{2,35} = 68.35$, p < 0.0001; diet: $F_{1,35} = 56.64$, p < 0.0001; week × diet: $F_{2,35} = 9.71$, $p = 0.00044$, n = 37) throughout the 4 weeks of control (CD)- or high-fat diet (HFD)-feeding, as well as stomach weight at the end of the experiment (time: $F_{2,31} = 139.24$, $p < 0.0001$; diet: $F_{1,31} = 0.035$, $p = 0.85$; time × diet: $F_{2,31} = 2.31$, $p = 0.12$, n = 37).

B. Representative microphotographs presenting spatial distribution of GLP1-immunoreactive fibres in relation to the different subdivisions of the DMH (c – compact, d – dorsal, v – ventral). 3 V – third ventricle, VMH – Ventromedial Hypothalamus.

C. Graphs presenting the results from the analysis of GLP1-positive fibres, performed for each DMH subdivision separately (diet: $F_{1,25} = 0.42$, $p = 0.52$; time: $F_{2,25} = 0.054$, $p = 0.95$; DMH div.: $F_{2,144} = 146.05$, $p < 0.0001$; diet × time: $F_{2,25} = 0.71$, p = 0.5; diet × DMH div.: $F_{2,144} = 0.76$, $p = 0.47$; time × DMH div.: $F_{4,144} = 0.96$, $p = 0.43$; diet × time × DMH: $F_{4,144} = 0.55$, $p = 0.7$; $n = 234$). BC—Box–Cox transformed values ($\lambda = 0.0202$).

D. Representative microphotographs presenting the density of cFos-positive cells depending on the time of meal onset and diet.

E. Graphs presenting the results from the analysis of the density of cFos-positive cells, performed for each DMH subdivision separately (diet: $F_{1,28} = 0.067$, p = 0.8; time: $F_{2,28} = 21.7$, p < 0.0001; DMH div.: $F_{2,170} = 104.37$, $p < 0.0001$; diet × time: $F_{2,28} = 1.2$, $p = 0.32$; diet × DMH div.: $F_{2,170} = 5.78$, $p = 0.0037$; time × DMH div.: $F_{4,170} = 3.96$, $p = 0.0042$; diet × time × DMH: $F_{4,170} = 2.16$, $p = 0.075$; $n = 273$). BC—Box–Cox transformed values ($\lambda = 0.3030$). *$p < 0.05$, **$p < 0.01$, ***$p < 0.001$, ****$p < 0.0001$. Box-and-whisker plots present the median value, the interquartile range (IQR; box) and the minimum-to-maximum range of values, not exceeding 1.5 * IQR (whiskers). Data points outside this range are plotted individually.

F. Representative microphotographs presenting colocalization of cFos and DAPI.

of expression, we analysed the mRNA density independently, where every fluorescent signal was included. In both cases, *Glp1r* showed very little expression in the cDMH. Surprisingly, even though the density of *Glp1r*-positive cells was higher in the dDMH than vDMH, signal density was equal between them, indicating higher *Glp1r* expression in fewer vDMH cells. Most importantly, we observed neither the general pattern, nor the level of expression of either receptor to change under HFD, despite literature presenting enhanced *Glp1r* expression in DIO (Zhang

et al., 2020). The fact that this gene is overexpressed in obesity, but not during its development could indicate that it is a result of the increased body mass, possibly as some form of a compensatory mechanism.

As for the distribution of the GLP1-positive neuronal fibres, our results are in line with others (Renner et al., 2012), showing the highest density within the vDMH, followed by the dDMH, with an observable gap in between. GLP1, GLP2 and Oxm are all products of one prohormone and are released from the same, PPG-expressing neurons

(Vrang et al., 2007), therefore the spatial pattern of GLP1 fibres observed by us will presumably also reflect that of the other PPG products. Indeed, the GLP2-positive fibres have also been observed mostly in the vDMH (Tang-Christensen et al., 2000).

The rationale for a separation of the DMH into the three outlined subdivisions is based on both molecular and functional characteristics. The cDMH has been postulated as a site for the local circadian oscillator, as the clock gene expression rhythm is the strongest within this part of the structure (Guilding et al., 2009). The vDMH seems to be the most involved with feeding-related cues (Poulin and Timofeeva, 2008; Kobelt et al., 2008; Renner et al., 2012) and transmitting the information to the master circadian clock in the Suprachiasmatic Nucleus (SCN, Acosta-Galvan et al., 2011). Last, the dDMH sends projections to the sympathetic premotor neurons in the rostral medullary raphe (Zhang et al., 2011; Kataoka et al., 2014), serving as a regulator of the thermogenesis and other autonomic nervous system functions (for a review see DiMicco and Zaretsky, 2007).

Indeed it was the vDMH which responded to feeding with the highest cFos expression, with the other two only doing so under restricted feeding. Feeding scheduled to regular, few-hour-long meals at the same time every day has been shown to alter DMH physiology increasing its circadian oscillatory properties, and switching phase depending on the meal time, so as to enable its anticipation (Mieda et al., 2006; Gooley et al., 2006; Verwey et al., 2007, 2008, 2009; Minana-Solis et al., 2009; Sanetra et al., 2022b). Our data indicate that this entrainment engages all three DMH subdivisions, as opposed to the vDMH simply responding to the post-meal satiety.

4.2. Exn4/Oxm/GLP2 influence on the DMH electrophysiology

Contrary to the receptor expression or fibre immunoreactivity, cells sensitive to the PPG-derived peptides were not restrained to any specific part of the structure. Moreover, despite a spatial separation in *Glp1r* and *Glp2r* expression, we spotted cells responsive to both Exn4 and GLP2, Oxm and GLP2, and even all three peptides. As far as the responsiveness to both Exn4 and Oxm did not surprise us, since both of these peptides bind GLP1R, either of them activating the same cell as GLP2 was unforeseen. Alternatively, the information delivered by these satiety signals is probably received by distinct neuronal subpopulations, but then spread across the entire structure via the synaptic network.

Regarding the peptides binding GLP1R, many of the recorded cells were indeed activated by both, but not all of them. Exn4 and Oxm have previously been shown to activate different hypothalamic structures (Chaudhri et al., 2006; Parkinson et al., 2009), suggesting a functional separation between them. Many of the neurons recorded in this study responded to Exn4 but not Oxm, possibly due to a higher affinity of Exn4 to the GLP1R (Baggio et al., 2004; Jorgensen et al., 2007). On the other hand, some neurons responded only to Oxm, which could also be explained as Oxm binds glucagon receptors (GCGR; Baldissera et al., 1988) in addition to GLP1R; however, GCGR expression in the DMH is questionable. Historically, many have failed to detect its presence in the entire brain completely, or found it to be generally low (Svoboda et al., 1994; Hansen et al., 1995), especially in the hypothalamus (Hoosein and Gurd, 1984). Others have spotted GCGR, with the highest density in the brainstem, only followed by the hypothalamus (Campos et al., 1994), but even within the hypothalamus the highest levels seem to occupy the Arcuate Nucleus and the Ventromedial Hypothalamus rather than the DMH (Quinones et al., 2015). This issue, however, remains to be clarified.

Acting through different receptors would also explain why some neurons responded differently to both peptides (i.e. an increase in the firing rate to one of them and a decrease to the other), however it is not the only explanation. Apart from the already mentioned possibility of a presynaptic influence, distinct intracellular pathways might be stimulated in the presence of different preferential allosteric ligands (Koole et al., 2010). The GLP1R is a complex protein with an ability to bind

various G proteins (Montrose-Rafizadeh et al., 1999), although the predominant mechanism involves the stimulation of adenyl cyclase by the G_α protein, which then induces phospholipase C activity via Epac2, leading to an increase in the intracellular Ca^{2+} concentration (Wheeler et al., 1993; Dzhura et al., 2010). Such pathway is extremely interesting to consider for the DMH, as our previous data indicate a presence of high-voltage activated (HVA) calcium channels, responsible for cells experiencing depolarised low-amplitude membrane oscillations (DLA-MOs) under strong depolarisation (Sanetra et al., 2022a) in this structure. The involvement of calcium channels activating at strong depolarisation seems a plausible mechanism also for the dependence of the response amplitude on baseline firing rate, indicative of the strength of depolarisation. Since this relationship completely disappears under HFD for both Exn4 and Oxm, it might be in fact these channels, rather than the receptors themselves, that become altered by the diet. On the other hand, L-type HVA calcium channels, participating in DLAMO generation in the SCN (Pennartz et al., 2002; Belle et al., 2009), have also been linked to the actions of GLP2R (Wang and Guan, 2010), which appeared unaffected by the diet. Additionally, a new study by Huang et al. (2022) suggests a different mechanism of the GLP1 action in the DMH, via a decrease in the delayed rectifier potassium current, causing cell depolarisation. However, in this patch clamp study no change in the firing rate was observed after Exn4 application, which is in contradiction to our results. We believe inconsistencies might stem from a different recording method (extracellular vs intracellular recording), and propose both mechanisms as plausible to mediate GLP1 effect on the DMH neurons. Interestingly, during our patch clamp recordings we failed to observe a postsynaptic effect on the neurons, which might be another argument for the necessity of a specific membrane potential for the signal transduction through voltage-gated channels.

A switch from regular, sodium-dependent spiking into slower DLA-MOs could also provide another explanation as to why some cells lowered their firing rate in response to the PPG-derived peptides. The fact that we observed a higher number of such neurons at night than during the day for all three peptides suggests a common underlying process. Whereas one option is of course the variation in the intensity of the GABAergic transmission, another could be related to the depolarisation above the threshold for DLAMOs or complete spiking blockage.

As suggested by the higher-than-expected number and a lack of spatial distribution of the cells responsive to Exn4/Oxm/GLP2, as well as verified with our patch clamp study, the DMH synaptic network is involved in signal transmission. For the GLP2 this was shown to differ between day and night, with a stronger decrease in the PSC frequency during the dark phase, which could also underlie the decrease in postsynaptic cells' firing rate more commonly observed at night. Same as for the MEA experiment, no effect of the diet was observed.

Also in line with the MEA results, the synaptic response to Exn4 was changed under HFD, in a form of an increased frequency of PSC during the day. Interestingly, we have previously observed an increased spontaneous firing rate during the light phase in the DMH (Sanetra et al., 2022b), which could be related to a malfunctioning of GLP1 signalling. On the other hand, the PSC response to Oxm application did not differ between either day/night or the diets, which once again indicates a distinct mechanism of action for the two GLP1R agonists.

It is important to note, that the investigation of the PSC frequency changes was performed in the absence of any specific synaptic blockers, or tetrodotoxin. The main rationale for these experiments was to confirm, that despite a moderate number of cells expressing the receptors for the PGDP, the ones which do, distribute this information throughout the structure resulting in an activation of about 40–50 % of the recorded cells. However, the investigation of the PGDP effect on the synaptic network functions, such as neurotransmitter release from the presynaptic terminal, would need to be addressed under pharmacological isolation. Further studies including a distinction of the type of current analysed (excitatory/inhibitory, type of ionic conductance), are needed to provide more in depth explanation on the nature of

phenomena observed.

4.3. GLP1 and cFos immunoreactivity under different metabolic states

The PPG family of peptides is responsible for satiety signalling; therefore, it could be assumed that their production as well as release is regulated by the animals' metabolic state. To explore that area, we studied the amount of GLP1 in the DMH by analysing GLP1-immunoreactive fibre density, under both hunger (48 h-long food deprivation) and satiety (2 h-long refeed). Since the DMH is well known for its entrainment to feeding schedules (Mieda et al., 2006; Gooley et al., 2006; Verwey et al., 2007, 2008, 2009; Minana-Solis et al., 2009; Sanetra et al., 2022b), we also applied a RF protocol (6 h long meal every night), which mimicked anticipated hunger/satiety. In order to monitor DMH cellular response to the same conditions, we also immunostained the cFos protein, as a marker of neuronal activity.

A 6 h-long mealtime was chosen as middle-length, when compared to others. While some researchers shorten it to 2 or 4 h (Gooley et al., 2006; Mieda et al., 2006; Verwey et al., 2007, 2008; Minana-Solis et al., 2009; Acosta-Rodríguez et al., 2022), far longer time windows are also common, even up to 8, 12 or 15 h (Hatori et al., 2012; Chaix et al., 2014; Vieira et al., 2022). In this case, we wanted to ensure the time restriction is strong enough to cause DMH anticipatory rhythms, while keeping the mealtime long enough to prevent caloric restriction, which could be an additional factor influencing the outcome of the study. Moreover, since the DMH had been observed to express day/night changes in cFos immunoreactivity (Gooley et al., 2006; Sanetra et al., 2022a), the meal onset was chosen as ZT14, so that the time point before the scheduled meal is also sampled during nighttime.

Throughout the CD/HFD feeding part of the experiment, the rats were weighed once a week. It was crucial to confirm that the HFD-fed group does not become significantly heavier than the controls at any point, since we were interested in studying potential mechanisms responsible for the development of obesity, rather than its consequences. Similarly to our previous reports (Chrobok et al., 2022; Sanetra et al., 2022b), an interaction between diet and week on a diet was observed, suggesting that the growth speed of the dietary groups differs, however up until the end of week 4, HFD-fed animals had not become heavier.

The fact that continuous body weight increase was present for both dietary groups throughout the experiment was related to the age of the animals at the start of it. Assigning the rats into CD- of HFD-fed groups, and the onset of specialist diet-feeding began at weaning, typically done at 4 weeks of age. Therefore, the rats at the time are still rapidly growing, which is well visible in the graphs presenting body mass changes from both FD and RF protocols. Our approach, aimed at modelling adolescent high-fat diet intake, does raise a question of how much the observed alterations, both behavioural and cellular, reflect also adult-onset obesity.

Also in line with previous reports, HFD-fed rats were shown to eat fewer grams of food, but more calories, due to the higher caloric value of the high-fat chow. Surprisingly though, the difference in the number of calories ingested during the 6 h window started declining immediately after RF onset and by the 4th week had completely vanished. On the other hand, our data on the 12 h-long RF did not follow the same trend, with an increased caloric intake throughout the entire experiment (Sanetra et al., 2022b). This discrepancy indicates meal length as an important factor determining the amount of food eaten, and suggests slower kinetics of the HFD consumption, additionally backed up by a lower density of cFos evoked 1.5 h after meal onset in the vDMH for the HFD group (Fig. 6E), as well as a slight (but not significant) trend implying lighter HFD stomachs at the same time point, despite lack of such difference before the meal, or 3.5 h after its onset (Fig. 6A). However, it is important to point out, that the HFD-fed animals decreased not only the caloric intake during the 2 weeks on the RF, but also total chow weight, indicating that the caloric restriction was voluntary, and the 6 h-long mealtime was enough for them to eat more,

had there been such a subjective need.

Previous studies revealed that food deprivation decreases the PPG neurons' activity (Maniscalco and Rinaman, 2013; Maniscalco et al., 2015) and GLP1 efficiency at inhibiting food intake (Sandoval et al., 2012). This was attributed to an interaction with feeding-related changes in the levels of circulating leptin (Williams et al., 2006). Consistently with these observations of a reduced GLP1 signalling in a fasted state, we found GLP1 fibre density to be lower under starvation and increase after refeeding. Interestingly, this dynamic was lost in animals fed HFD. In the vDMH the satiety-induced GLP1 immunofluorescence failed to reach such a high level, whereas in the dDMH higher GLP1 density was observed during FD. This second result is particularly surprising, but might point to differences in the hunger-related metabolic processes, regulated by this part of the structure.

On the other hand, under RF the GLP1 fibre density remained unchanged by the scheduled meal. The reason for it might be the lack of FD-caused drop due to a shorter time window without any food during the RF protocol in comparison with the 48 h starvation. However, the stomachs weighed very similarly at the end of both protocols regarding the hungry groups. Instead, the lack of changes might also indicate meal anticipation in a form of neuronal terminals storing GLP1 so as to enable a swift response to the scheduled feeding.

Importantly, GLP1 fibre immunoreactivity was constant across the feeding cycle also for the HFD-fed rats, neither did it differ between the diets at any time point. Scheduled feeding has been proven beneficial for longevity (Acosta-Rodríguez et al., 2022), as well as metabolic health, even capable of preventing obesity altogether (Hatori et al., 2012; Sherman et al., 2012; Chaix et al., 2014; Vieira et al., 2022). Lately, we have also shown that 12 h-long RF can prevent the disturbance in the DMH circadian clock (Sanetra et al., 2022b). Results presented in this article provide another example of the advantageous influence of time-restricted feeding.

Concluding, in this study we investigated PPG signalling in the DMH, confirming the presence and specific spatial distribution of GLP1-positive neuronal fibres, GLP1 and GLP2 receptors, as well as investigated Exn4/Oxm/GLP2 influence on the DMH neurons and the synaptic network. Most importantly, our results provide an insight into HFD-mediated changes in the PPG signalling on two distinct levels: disrupted feeding-related dynamics of GLP1 density in the structure, and altered neuronal responsiveness to the GLP1R agonists, despite a lack of change in the receptor expression. Presented study is an important step towards understanding PPG signalling in the brain, especially vital with the view of an already wide usage of GLP1R agonists in therapy.

Funding

CRediT authorship contribution statement

A.M. Sanetra: Conceptualization, Data curation, Formal analysis, Investigation, Methodology, Visualization, Writing – original draft. **K. Palus-Chramiec:** Conceptualization, Data curation, Formal analysis, Investigation, Methodology, Writing – review & editing. **L. Chrobok:** Conceptualization, Data curation, Formal analysis, Investigation, Methodology, Writing – review & editing. **J.S. Jeczmien-Lazur:** Conceptualization, Investigation, Methodology, Writing – review & editing. **J.D. Klich:** Investigation, Writing – review & editing. **M.H. Lewandowski:** Conceptualization, Funding acquisition, Project administration, Resources, Supervision, Writing – review & editing.

Declaration of competing interest

Authors declare no conflict of interests.

Data availability

The data presented in this study are available upon request.

Acknowledgements

We would like to thank Patrycjusz Nowik for excellent animal care.

Appendix A. Supplementary data

Supplementary data to this article can be found online at https://doi.org/10.1016/j.mcn.2023.103873.

References

Acosta-Galvan, G., Yi, C.X., van der Vliet, J., Jhamandas, J.H., Panula, P., Angeles-Castellanos, M., Buijs, R.M., 2011. Interaction between hypothalamic dorsomedial nucleus and the suprachiasmatic nucleus determines intensity of food anticipatory behavior. Proc. Natl. Acad. Sci. 108 (14), 5813–5818.

Acosta-Rodríguez, V., Rijo-Ferreira, F., Izumo, M., Xu, P., Wight-Carter, M., Green, C.B., Takahashi, J.S., 2022. Circadian alignment of early onset caloric restriction promotes longevity in male C57BL/6J mice. Science 376 (6598), 1192–1202.

Baggio, L.L., Huang, Q., Brown, T.J., Drucker, D.J., 2004. Oxyntomodulin and glucagon-like peptide-1 differentially regulate murine food intake and energy expenditure. Gastroenterology 127 (2), 546–558.

Baldissera, F.G., Holst, J.J., Knuhtsen, S., Hilsted, L., Nielsen, O.V., 1988. Oxyntomodulin (glicentin-(33–69)): pharmacokinetics, binding to liver cell membranes, effects on isolated perfused pig pancreas, and secretion from isolated perfused lower small intestine of pigs. Regul. Pept. 21 (1–2), 151–166.

Bataille, D., Dalle, S., 2014. The forgotten members of the glucagon family. Diabetes Res. Clin. Pract. 106 (1), 1–10.

Bates, D., Maechler, M., Bolker, B.M., Walker, S., 2015. Fitting linear mixed-effects models using lme4. J. Stat. Softw. 67, 1–48.

Belle, M.D., Diekman, C.O., Forger, D.B., Piggins, H.D., 2009. Daily electrical silencing in the mammalian circadian clock. Science 326 (5950), 281–284.

Belle, M.D., Baño-Otalora, B., Piggins, H.D., 2021. Perforated multi-electrode array recording in hypothalamic brain slices. In: Circadian Clocks. Humana, New York, NY, pp. 263–285.

Box, G.E.P., Cox, D.R., 1964. An analysis of transformations. J. R. Stat. Soc. Ser. B 26, 211–252.

Campos, R.V., Lee, Y.C., Drucker, D.J., 1994. Divergent tissue-specific and developmental expression of receptors for glucagon and glucagon-like peptide-1 in the mouse. Endocrinology 134 (5), 2156–2164.

Chaix, A., Zarrinpar, A., Miu, P., Panda, S., 2014. Time-restricted feeding is a preventative and therapeutic intervention against diverse nutritional challenges. Cell Metab. 20 (6), 991–1005.

Chaudhri, O.B., Parkinson, J.R., Kuo, Y.T., Druce, M.R., Herlihy, A.H., Bell, J.D., Bloom, S.R., 2006. Differential hypothalamic neuronal activation following peripheral injection of GLP-1 and oxyntomodulin in mice detected by manganese-enhanced magnetic resonance imaging. Biochem. Biophys. Res. Commun. 350 (2), 298–306.

Chrobok, L., Klich, J.D., Sanetra, A.M., Jeczmien-Lazur, J.S., Pradel, K., Palus-Chramiec, K., Lewandowski, M.H., 2022. Rhythmic neuronal activities of the rat nucleus of the solitary tract are impaired by high-fat diet–implications for daily control of satiety. J. Physiol. 600 (4), 751–767.

Cork, S.C., Richards, J.E., Holt, M.K., Gribble, F.M., Reimann, F., Trapp, S., 2015. Distribution and characterisation of glucagon-like peptide-1 receptor expressing cells in the mouse brain. Molecular metabolism 4 (10), 718–731.

Dakin, C.L., Gunn, I., Small, C.J., Edwards, C.M.B., Hay, D.L., Smith, D.M., Bloom, S.R., 2001. Oxyntomodulin inhibits food intake in the rat. Endocrinology 142 (10), 4244–4250.

Dakin, C.L., Small, C.J., Park, A.J., Seth, A., Ghatei, M.A., Bloom, S.R., 2002. Repeated ICV administration of oxyntomodulin causes a greater reduction in body weight gain than in pair-fed rats. American Journal of Physiology-Endocrinology and Metabolism 283 (6), E1173–E1177.

DiMicco, J.A., Zaretsky, D.V., 2007. The dorsomedial hypothalamus: a new player in thermoregulation. Am. J. Phys. Regul. Integr. Comp. Phys. 292 (1), R47–R63.

Dupré, J., Behme, M.T., McDonald, T.J., 2004. Exendin-4 normalized postcibal glycemic excursions in type 1 diabetes. The journal of clinical endocrinology & metabolism 89 (7), 3469–3473.

Dzhura, I., Chepurny, O.G., Kelley, G.G., Leech, C.A., Roe, M.W., Dzhura, E., Holz, G.G., 2010. Epac2-dependent mobilization of intracellular Ca2+ by glucagon-like peptide-1 receptor agonist exendin-4 is disrupted in β-cells of phospholipase C-ε knockout mice. J. Physiol. 588 (24), 4871–4889.

Fox, J., Weisberg, S., 2019. An R Companion to Applied Regression. Sage Publications. https://socialsciences.mcmaster.ca/jfox/Books/Companion/.

Gooley, J.J., Schomer, A., Saper, C.B., 2006. The dorsomedial hypothalamic nucleus is critical for the expression of food-entrainable circadian rhythms. Nat. Neurosci. 9 (3), 398–407.

Guilding, C., Hughes, A.T., Brown, T.M., Namvar, S., Piggins, H.D., 2009. A riot of rhythms: neuronal and glial circadian oscillators in the mediobasal hypothalamus. Molecular brain 2 (1), 1–19.

Hansen, L.H., Abrahamsen, N., Nishimura, E., 1995. Glucagon receptor mRNA distribution in rat tissues. Peptides 16 (6), 1163–1166.

Hatori, M., Vollmers, C., Zarrinpar, A., DiTacchio, L., Bushong, E.A., Gill, S., Panda, S., 2012. Time-restricted feeding without reducing caloric intake prevents metabolic diseases in mice fed a high-fat diet. Cell Metab. 15 (6), 848–860.

Hoosein, N.M., Gurd, R.S., 1984. Identification of glucagon receptors in rat brain. Proc. Natl. Acad. Sci. 81 (14), 4368–4372.

Huang, Z., Liu, L., Zhang, J., Conde, K., Phansalkar, J., Li, Z., Liu, J., 2022. Glucose-sensing glucagon-like peptide-1 receptor neurons in the dorsomedial hypothalamus regulate glucose metabolism. Science Advances 8 (23), eabn5345.

Hwa, J.J., Ghibaudi, L., Williams, P., Witten, M.B., Tedesco, R., Strader, C.D., 1998. Differential effects of intracerebroventricular glucagon-like peptide-1 on feeding and energy expenditure regulation. Peptides 19 (5), 869–875.

Jorgensen, R., Kubale, V., Vrecl, M., Schwartz, T.W., Elling, C.E., 2007. Oxyntomodulin differentially affects glucagon-like peptide-1 receptor β-arrestin recruitment and signaling through Gα. J. Pharmacol. Exp. Ther. 322 (1), 148–154.

Kassambara, A., 2020. ggpubr: 'ggplot2' Based Publication Ready Plots. R package version 0.4.0. https://CRAN.R-project.org/package=ggpubr.

Kassambara, A., 2021. rstatix: Pipe-Friendly Framework for Basic Statistical Tests. R package version 0.7.0. https://CRAN.R-project.org/package=rstatix.

Kataoka, N., Hioki, H., Kaneko, T., Nakamura, K., 2014. Psychological stress activates a dorsomedial hypothalamus-medullary raphe circuit driving brown adipose tissue thermogenesis and hyperthermia. Cell Metab. 20 (2), 346–358.

Kobelt, P., Wisser, A.S., Stengel, A., Goebel, M., Inhoff, T., Noetzel, S., Mönnikes, H., 2008. Peripheral injection of ghrelin induces Fos expression in the dorsomedial hypothalamic nucleus in rats. Brain Res. 1204, 77–86.

Kolterman, O.G., Buse, J.B., Fineman, M.S., Gaines, E., Heintz, S., Bicsak, T.A., Baron, A. D., 2003. Synthetic exendin-4 (exenatide) significantly reduces postprandial and fasting plasma glucose in subjects with type 2 diabetes. The Journal of Clinical Endocrinology & Metabolism 88 (7), 3082–3089.

Koole, C., Wootten, D., Simms, J., Valant, C., Sridhar, R., Woodman, O.L., Sexton, P.M., 2010. Allosteric ligands of the glucagon-like peptide 1 receptor (GLP-1R) differentially modulate endogenous and exogenous peptide responses in a pathway-selective manner: implications for drug screening. Mol. Pharmacol. 78 (3), 456–465.

Kosinski, J.R., Hubert, J., Carrington, P.E., Chicchi, G.G., Mu, J., Miller, C., Pocai, A., 2012. The glucagon receptor is involved in mediating the body weight-lowering effects of oxyntomodulin. Obesity 20 (8), 1566–1571.

Kunzetsova, A., Brockhoff, P., Christensen, R., 2017. lmerTest package: tests in linear mixed effect models. J. Stat. Softw. 82, 1–26.

Larsen, P.J., Tang-Christensen, M., Holst, J.J., Ørskov, C., 1997. Distribution of glucagon-like peptide-1 and other preproglucagon-derived peptides in the rat hypothalamus and brainstem. Neuroscience 77 (1), 257–270.

Lee, S.J., Sanchez-Watts, G., Krieger, J.P., Pignalosa, A., Norell, P.N., Cortella, A., Watts, A.G., 2018. Loss of dorsomedial hypothalamic GLP-1 signaling reduces BAT thermogenesis and increases adiposity. Molecular metabolism 11, 33–46.

Lenth, R.V., 2021. emmeans: Estimated Marginal Means, aka Least-Squares Means. R package version 1.5.5-1. https://CRAN.R-project.org/package=emmeans.

Maejima, Y., Yokota, S., Shimizu, M., Horita, S., Kobayashi, D., Hazama, A., Shimomura, K., 2021. The deletion of glucagon-like peptide-1 receptors expressing neurons in the dorsomedial hypothalamic nucleus disrupts the diurnal feeding pattern and induces hyperphagia and obesity. Nutrition & metabolism 18 (1), 1–15.

Maniscalco, J.W., Rinaman, L., 2013. Overnight food deprivation markedly attenuates hindbrain noradrenergic, glucagon-like peptide-1, and hypothalamic neural responses to exogenous cholecystokinin in male rats. Physiol. Behav. 121, 35–42.

Maniscalco, J.W., Zheng, H., Gordon, P.J., Rinaman, L., 2015. Negative energy balance blocks neural and behavioral responses to acute stress by "silencing" central glucagon-like peptide 1 signaling in rats. J. Neurosci. 35 (30), 10701–10714.

Merchenthaler, I., Lane, M., Shughrue, P., 1999. Distribution of pre-pro-glucagon and glucagon-like peptide-1 receptor messenger RNAs in the rat central nervous system. J. Comp. Neurol. 403 (2), 261–280.

Mieda, M., Williams, S.C., Richardson, J.A., Tanaka, K., Yanagisawa, M., 2006. The dorsomedial hypothalamic nucleus as a putative food-entrainable circadian pacemaker. Proc. Natl. Acad. Sci. 103 (32), 12150–12155.

Minana-Solis, M.C., Angeles-Castellanos, M., Feillet, C., Pevet, P., Challet, E., Escobar, C., 2009. Differential effects of a restricted feeding schedule on clock-gene expression in the hypothalamus of the rat. Chronobiol. Int. 26 (5), 808–820.

Montrose-Rafizadeh, C., Avdonin, P., Garant, M.J., Rodgers, B.D., Kole, S., Yang, H., Bernier, M., 1999. Pancreatic glucagon-like peptide-1 receptor couples to multiple G proteins and activates mitogen-activated protein kinase pathways in Chinese hamster ovary cells. Endocrinology 140 (3), 1132–1140.

Osaka, T., Endo, M., Yamakawa, M., Inoue, S., 2005. Energy expenditure by intravenous administration of glucagon-like peptide-1 mediated by the lower brainstem and sympathoadrenal system. Peptides 26 (9), 1623–1631.

Pachitariu, M., Steinmetz, N., Kadir, S., Carandini, M., Harris, K.D., 2016. Kilosort: realtime spike-sorting for extracellular electrophysiology with hundreds of channels. bioRxiv, 061481. https://doi.org/10.1101/061481.

Parkinson, J.R., Chaudhri, O.B., Kuo, Y.T., Field, B.C., Herlihy, A.H., Dhillo, W.S., Bell, J. D., 2009. Differential patterns of neuronal activation in the brainstem and hypothalamus following peripheral injection of GLP-1, oxyntomodulin and lithium chloride in mice detected by manganese-enhanced magnetic resonance imaging (MEMRI). Neuroimage 44 (3), 1022–1031.

Pennartz, C.M., de Jeu, M.T., Bos, N.P., Schaap, J., Geurtsen, A.M., 2002. Diurnal modulation of pacemaker potentials and calcium current in the mammalian circadian clock. Nature 416 (6878), 286–290.

Pocai, A., Carrington, P.E., Adams, J.R., Wright, M., Eiermann, G., Zhu, L., SinhaRoy, R., 2009. Glucagon-like peptide 1/glucagon receptor dual agonism reverses obesity in mice. Diabetes 58 (10), 2258–2266.

Poulin, A.M., Timofeeva, E., 2008. The dynamics of neuronal activation during food anticipation and feeding in the brain of food-entrained rats. Brain Res. 1227, 128–141.

Quinones, M., Al-Massadi, O., Gallego, R., Fernø, J., Diéguez, C., López, M., Nogueiras, R., 2015. Hypothalamic CaMKKβ mediates glucagon anorectic effect and its diet-induced resistance. Molecular metabolism 4 (12), 961–970.

Renner, E., Puskas, N., Dobolyi, A., Palkovits, M., 2012. Glucagon-like peptide-1 of brainstem origin activates dorsomedial hypothalamic neurons in satiated rats. Peptides 35 (1), 14–22.

Sandoval, D., Barrera, J.G., Stefater, M.A., Sisley, S., Woods, S.C., D'Alessio, D.D., Seeley, R.J., 2012. The anorectic effect of GLP-1 in rats is nutrient dependent. PLoS One 7 (12), e51870.

Sanetra, A.M., Palus-Chramiec, K., Chrobok, L., Lewandowski, M.H., 2022a. Electrophysiological complexity in the rat dorsomedial hypothalamus and its susceptibility to daily rhythms and high-fat diet. Eur. J. Neurosci. 56 (4), 4363–4377.

Sanetra, A.M., Palus-Chramiec, K., Chrobok, L., Jeczmien-Lazur, J.S., Gawron, E., Klich, J.D., Lewandowski, M.H., 2022b. High-fat-diet-evoked disruption of the rat dorsomedial hypothalamic clock can be prevented by restricted nighttime feeding. Nutrients 14 (23), 5034.

Schindelin, J., Arganda-Carreras, I., Frise, E., Kaynig, V., Longair, M., Pietzsch, T., Cardona, A., 2012. Fiji: an open-source platform for biological-image analysis. Nat. Methods 9 (7), 676–682.

Sherman, H., Genzer, Y., Cohen, R., Chapnik, N., Madar, Z., Froy, O., 2012. Timed high-fat diet resets circadian metabolism and prevents obesity. FASEB J. 26 (8), 3493–3502.

Svoboda, M., Tastenoy, M., Vertongen, P., Robberecht, P., 1994. Relative quantitative analysis of glucagon receptor mRNA in rat tissues. Mol. Cell. Endocrinol. 105 (2), 131–137.

Tang-Christensen, M., Larsen, P.J., Thulesen, J., Rømer, J., Vrang, N., 2000. The proglucagon-derived peptide, glucagon-like peptide-2, is a neurotransmitter involved in the regulation of food intake. Nat. Med. 6 (7), 802–807.

Tang-Christensen, M., Vrang, N., Larsen, P.J., 2001. Glucagon-like peptide containing pathways in the regulation of feeding behaviour. Int. J. Obes. 25 (5), S42–S47.

Team, R., 2015. 2019. Integrated Development for R. RStudio, Inc., Boston, MA, RStudio. http://www.rstudio.com/.

Team, R.C., 2021. R: A Language and Environment for Statistical Computing. R Foundation for Statistical Computing, Vienna, Austria. https://www.R-project.org/.

Trujillo, J.M., Nuffer, W., Smith, B.A., 2021. GLP-1 receptor agonists: an updated review of head-to-head clinical studies. In: Therapeutic Advances in Endocrinology and Metabolism, 12, 2042018821997320.

Venables, W.N., Ripley, B.D., 2002. Modern Applied Statistics with S, , Fourth edition53. World, p. 578.

Verwey, M., Khoja, Z., Stewart, J., Amir, S., 2007. Differential regulation of the expression of Period2 protein in the limbic forebrain and dorsomedial hypothalamus by daily limited access to highly palatable food in food-deprived and free-fed rats. Neuroscience 147 (2), 277–285.

Verwey, M., Khoja, Z., Stewart, J., Amir, S., 2008. Region-specific modulation of PER2 expression in the limbic forebrain and hypothalamus by nighttime restricted feeding in rats. Neurosci. Lett. 440 (1), 54–58.

Verwey, M., Lam, G.Y., Amir, S., 2009. Circadian rhythms of PERIOD1 expression in the dorsomedial hypothalamic nucleus in the absence of entrained food-anticipatory activity rhythms in rats. Eur. J. Neurosci. 29 (11), 2217–2222.

Vieira, R.F.L., Muñoz, V.R., Junqueira, R.L., de Oliveira, F., Gaspar, R.C., Nakandakari, S. C.B.R., Pauli, J.R., 2022. Time-restricted feeding combined with aerobic exercise training can prevent weight gain and improve metabolic disorders in mice fed a high-fat diet. J. Physiol. 600 (4), 797–813.

Vrang, N., Hansen, M., Larsen, P.J., Tang-Christensen, M., 2007. Characterization of brainstem preproglucagon projections to the paraventricular and dorsomedial hypothalamic nuclei. Brain Res. 1149, 118–126.

Wang, Y., Guan, X., 2010. GLP-2 potentiates L-type Ca2+ channel activity associated with stimulated glucose uptake in hippocampal neurons. American Journal of Physiology-Endocrinology and Metabolism 298 (2), E156–E166.

Wheeler, M.B., Lu, M.I.N.G., Dillon, J.S., Leng, X.H., Chen, C.H.U.A.N., Boyd 3rd, A.E., 1993. Functional expression of the rat glucagon-like peptide-I receptor, evidence for coupling to both adenylyl cyclase and phospholipase-C. Endocrinology 133 (1), 57–62.

Williams, D.L., Baskin, D.G., Schwartz, M.W., 2006. Leptin regulation of the anorexic response to glucagon-like peptide-1 receptor stimulation. Diabetes 55 (12), 3387–3393.

Winzell, M.S., Ahrén, B., 2004. The high-fat diet–fed mouse: a model for studying mechanisms and treatment of impaired glucose tolerance and type 2 diabetes. Diabetes 53 (suppl_3), S215–S219.

Wynne, K., Park, A.J., Small, C.J., Meeran, K., Ghatei, M.A., Frost, G.S., Bloom, S.R., 2006. Oxyntomodulin increases energy expenditure in addition to decreasing energy intake in overweight and obese humans: a randomised controlled trial. Int. J. Obes. 30 (12), 1729–1736.

Zhang, C., Barkholt, P., Nielsen, J.C., Thorbek, D.D., Rigbolt, K., Vrang, N., Jelsing, J., 2020. The dorsomedial hypothalamus and nucleus of the solitary tract as key regulators in a rat model of chronic obesity. Brain Res. 1727, 146538.

Zhang, Y., Kerman, I.A., Laque, A., Nguyen, P., Faouzi, M., Louis, G.W., Münzberg, H., 2011. Leptin-receptor-expressing neurons in the dorsomedial hypothalamus and median preoptic area regulate sympathetic brown adipose tissue circuits. J. Neurosci. 31 (5), 1873–1884.